Biomaterials 98 (2016) 192–202

Contents lists available at ScienceDirect

Biomaterials

journal homepage: www.elsevier.com/locate/biomaterials

MMP-9 triggered self-assembly of doxorubicin nanofiber depots halts tumor growth

Daniela Kalafatovic [a, **, 1], Max Nobis [b, 1], Jiye Son [a, e], Kurt I. Anderson [b, f, ***], Rein V. Ulijn [a, c, d, e, *]

[a] Advanced Science Research Center (ASRC), City University New York, 85 St Nicholas Terrace, New York, NY 10031, USA
[b] CRUK Beatson Institute, Garscube Estate, Glasgow, G61 1BD, UK
[c] WestCHEM, Department of Pure and Applied Chemistry, University of Strathclyde, 295 Cathedral Street, Glasgow, G1 1XL, UK
[d] Department of Chemistry and Biochemistry, City University of New York – Hunter College, 695 Park Ave., New York, NY 10065, USA
[e] The Graduate Center of the City University of New York, New York, NY 10016, USA
[f] The Francis Crick Institute, 215 Euston Road, London NW1 2BE, UK

ARTICLE INFO

Article history:
Received 21 January 2016
Received in revised form
18 April 2016
Accepted 28 April 2016
Available online 30 April 2016

Keywords:
Peptides
Self-assembly
MMP
Cancer therapy
Morphology transition

ABSTRACT

A central challenge in cancer care is to ensure that therapeutic compounds reach their targets. One approach is to use enzyme-responsive biomaterials, which reconfigure in response to endogenous enzymes that are overexpressed in diseased tissues, as potential site-specific anti-tumoral therapies. Here we report peptide micelles that upon MMP-9 catalyzed hydrolysis reconfigure to form fibrillar nanostructures. These structures slowly release a doxorubicin payload at the site of action. Using both *in vitro* and *in vivo* models, we demonstrate that the fibrillar depots are formed at the sites of MMP-9 overexpression giving rise to enhanced efficacy of doxorubicin, resulting in inhibition of tumor growth in an animal model.

1. Introduction

Cancer nanomedicines have the potential to lead to innovative drug formulation strategies through the design of nanocarriers that improve efficacy and bioavailability, incorporate targeting opportunities and may lead to personalization as well as increased safety compared to conventional medicines [1–3]. Development of successful cancer nanomedicines has been hindered, however, due to the lack of target specificity [4]. Nevertheless, some examples of anti-cancer nanomedicines have reached the clinic. Currently approved treatments include doxorubicin loaded PEGylated liposome formulations (Doxil) for the treatment of ovarian cancer and Karposi's sarcoma [4,5] and paclitaxel/albumin nanoparticles (Abraxane) for the treatment of metastatic breast cancer [6,7]. These existing and other emerging [8] nanoformulations are designed to enhance circulation of poorly soluble chemotherapeutics. Other approaches are focused on injecting polymer formulations at the tumor site, to create depots that enable localized drug delivery [9].

As alternatives to lipids or polymers, peptide nanostructures are attractive for biomedical applications [10–13] due to their chemical versatility and the GRAS (generally recognized as safe) status (21CFR72.320) of their amino acid breakdown products. One example which is currently being assessed for clinical use are peptide nanofiber scaffolds (PuraMatrix) for tissue engineering, drug delivery and regenerative medicine [14,15]. In the current work, we aim to generate liposome-like peptide nanocarriers able to autonomously form nanofibrous peptide depots at the tumor site in response to enzymes secreted by cancer cells.

Targeting the enzymes that are over-expressed in cancer sites provides a route towards more specific cancer nanocarriers [16–18]. In particular, a number of enzyme-responsive supramolecular materials have been developed that change their morphology upon

* Corresponding author. Advanced Science Research Center (ASRC), City University New York, 85 St Nicholas Terrace, New York, NY 10031, USA.
** Corresponding author.
*** Corresponding author. CRUK Beatson Institute, Garscube Estate, Glasgow, G61 1BD, UK.
E-mail addresses: daniela.kalafatovic@irbbarcelona.org (D. Kalafatovic), kurt.anderson@crick.ac.uk (K.I. Anderson), Rein.Ulijn@asrc.cuny.edu (R.V. Ulijn).
[1] These authors contributed equally.

http://dx.doi.org/10.1016/j.biomaterials.2016.04.039

enzyme action [19–24]. Matrix-metalloproteinases (MMPs) are over-expressed in many types of cancer and are involved in metastasis formation due to their ability to degrade the extracellular matrix [25,26]. Due to this cancer-specific overexpression, the enzymatic activity of MMPs provides opportunities to manage or report cancer progression autonomously and only when and where it is required [20,21,27–30]. MMPs are therefore logical targets for enzyme-triggered therapeutics.

A variety of supramolecular assemblies (such as peptide amphiphiles [21,31–33] and polymer-peptide hybrids [34]) have been developed that dissociate in response to MMP action. Typically, these nanocarrier designs include a hydrophobic core that holds the drug, which is then released in response to the MMP catalyzed breakdown of the carrier. In an alternative approach, enzymatic triggering by cell surface bound enzymes (phosphatases) results in the formation of supramolecular nanofiber networks, providing localized barriers around cancer cells that result in cell death [22,35,36]. Enzyme-triggered morphology changes have been used to drive the formation of aggregated, amorphous materials, which selectively accumulate and retain polymer-peptide conjugates in tumor tissues [20,37]. Recently, a combination therapy consisting of enzyme (carboxylesterase) triggered peptide fibrillization combined with an anticancer drug (cisplatin) was shown to dramatically enhance drug toxicity against drug-resistant cells [38].

The above examples clearly illustrate that supramolecular peptide structures are well-suited to achieve enzyme-triggered morphology transitions. We propose that the peptides may be designed that combine a number of features of the above examples into one system: (1) the peptides should form micelles with hydrophobic cores that can contain doxorubicin; (2) they should be hydrolysable by MMP-9; (3) upon hydrolysis the amphiphilic balance should shift so that nanofibers are formed, which incorporate the doxorubicin (Fig. 1). This would allow for the formation of micelles as mobile nanocarriers, which form localized depots in areas where cancer-specific enzymes are secreted.

We designed our system by following design rules for MMP-9 specificity (MEROPS) in combination with the incorporation of short β-sheet forming peptides (composed of just four-six amino acids) into the MMP-9 substrate. In this way, hydrophobic pockets (xFFyG, where x is either glycine or phenylacetyl group and y is leucine or alanine) for doxorubicin entrapment and MMP-9 substrates are incorporated in the nanocarrier structure. In order to test whether these systems can indeed perform as autonomously localized release systems (Fig. 1) both *in vitro* and *in vivo* tests were performed. Ultimately, by using a xenograft mouse model, we show that localized formation of doxorubicin-containing fibers slows tumor growth compared to treatment with doxorubicin only. Our approach uses a pathological hallmark of metastasis (MMP overexpression) to guide therapeutic targeting, thereby turning a negative prognostic indicator into a therapeutic response.

2. Materials and methods

2.1. Peptide synthesis

All peptides where synthesized using standard Fmoc solid phase peptide synthesis on Wang resin pre-loaded with the first amino acid. Amino acid coupling was performed with a three-fold excess of the Fmoc protected amino acid over the resin in DMF, using N,N,N′,N′-Tetramethyl-O-(1H-benzotriazol-1-yl) uronium hexafluorophosphate (HBTU) and *N*,*N*-Diisopropylethylamine (DIPEA) as activating and coupling reagents in 1:2 ratio respectively relative to the amino acid. Fmoc removal was carried out with 20% piperidine in DMF. The cleavage of the peptides from the resin was achieved using a cleavage cocktail: 95% TFA, 2.5% triisopropylsilane (TIS), and 2.5% water. The crude peptide was precipitated and washed in cold diethyl ether and subsequently dissolved in water to allow further purification. For the dissolution of hydrophobic sequences minimal amount of acetonitrile was used to ease the dissolution of any non-dissolved material (in water). The samples were then characterized by reverse phase high-performance liquid chromatography (HPLC) and liquid chromatography-mass spectrometry (LCMS) to determine the purity and M_w of the product. The peptides were purified by Almac Sciences (Elvingston Science Center, Gladsmuir, East Lothian, Edinburgh, EH33 1EH, Scotland).

2.2. Nanostructure formation and characterization

The micelle forming peptide **2a** was directly dissolved in deionized water, the pH adjusted to 7.4 and its self-assembly behavior investigated after a cycle of alternating sonication and vortexing. For the expected enzyme cleavage peptide fragment i.e. **2b** and the observed cleavage product (**2c**) the peptides were dissolved in deionized water and the pH was increased (NaOH 0.5 M) to solubilize **2b/2c**, followed by a slow decrease of pH achieved by addition of HCl 0.5 M, to a final pH of 6.5–7 to trigger gelation. Gelation was observed for the expected MMP-9 cleavage product **2b** and for the observed cleavage product **2c**. Incorporation of doxorubicin was achieved by solubilizing in DMSO by sonication and a 1 mM stock solution in PBS was made and subsequent dilution into a suspension of peptide micelles.

2.3. Atomic force microscopy

AFM was performed using a Bruker, NanoScope V, Multimode 8 atomic force microscope. The samples were placed on a trimmed and freshly cleaved mica sheet (G250-2 Mica sheets 1" × 1" × 0.006") attached to an AFM support stub and left to air-dry overnight in a dust-free environment, prior to imaging. All the images were obtained using ScanAsyst in air mode. The resolution of the scans is 512 × 512 pixels. Typical scanning speed was 1.0 Hz. The images were analysed using NanoScope Analysis software Version 1.50.

2.4. Transmission electron microscopy

TEM imaging was performed at the Advanced Science Research Center (ASRC), CUNY Imaging Facility using a FEI, TITAN Halo transmission electron microscope operating at 300 kV fitted with CETA 4 K × 4 K camera. Carbon-coated copper grids (200 mesh) were glow discharged in air for 30 s. 5 μL of sample was added to the grid and blotted down using filter paper after 60 s. For double staining, a negative stain (2% aqueous uranyl acetate) was applied twice (30 s each time) and the mixture blotted again using filter paper to remove excess. The dried specimens were then imaged.

2.5. Scanning electron microscopy

SEM imaging was performed at the University of Glasgow Electron Microscopy facility. Cells were allowed to adhere on previously sterilized glass coverslips, serum starved overnight and treated with 100 nM PMA to induce MMP-9 production. Then, they were treated with 2.5 mM of peptide **2a** for 72 h. After peptide treatment, the cells were fixed on glass coverslips using 1.5% glutaraldehyde in 0.1 M sodium cacodylate buffer (1 h at 4 °C). The cells were then freeze-dried in liquid nitrogen. Samples were subsequently sputter coated with gold (8 nm thick coating) under vacuum and imaged using a JEOL-JSM 6400 field emission scanning electron microscope operated at an acceleration voltage of 10 kV.

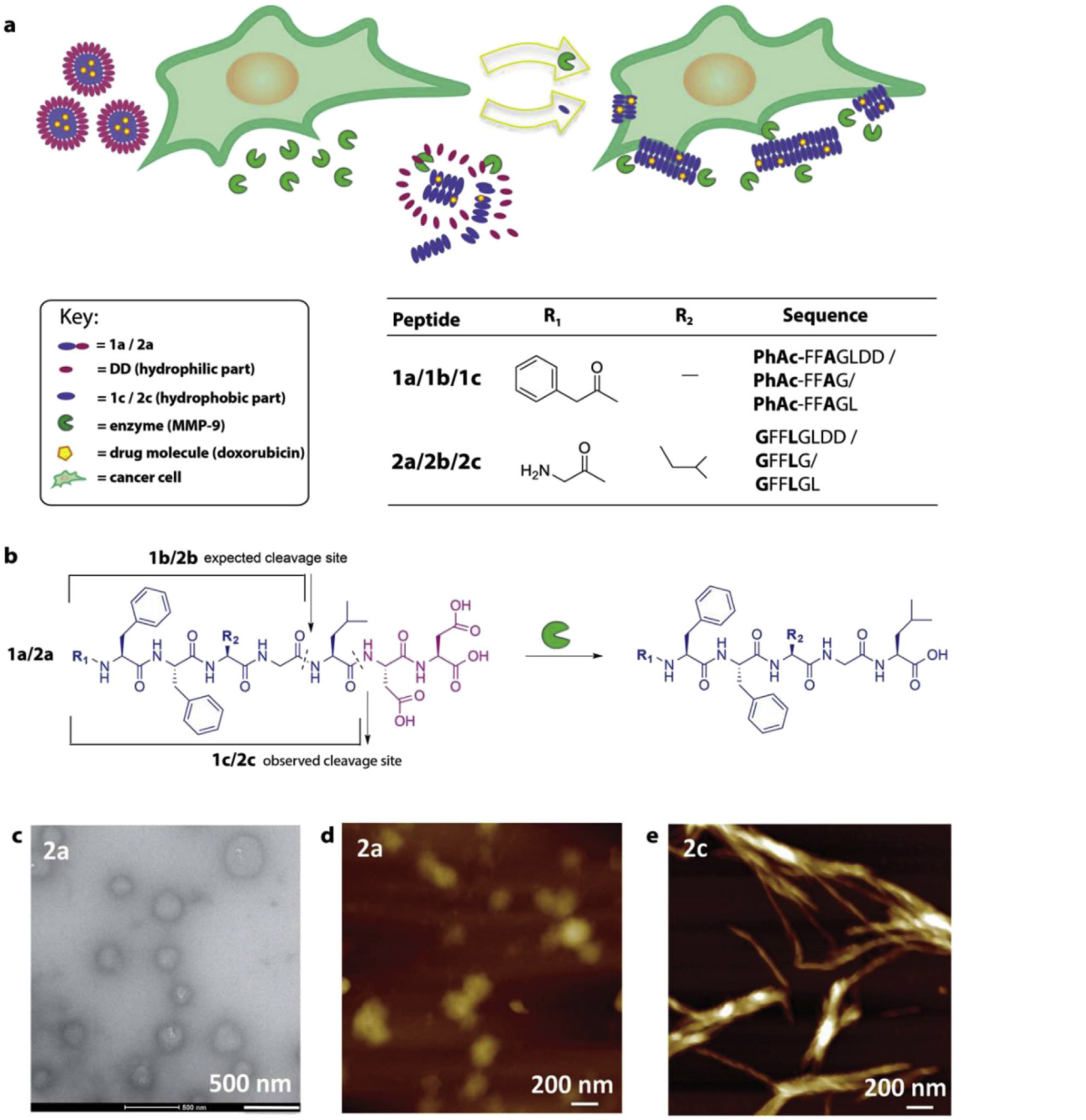

Fig. 1. MMP-9 triggered micelle to fiber transition. (**a**) Schematic representation of micelle-to-fiber transition in the presence of cancer cells due to MMP-9 secretion, followed by entrapment of doxorubicin in fibrillar structures, which act as less mobile depots of the anticancer drug. (**b**) Chemical structure of the MMP-9 responsive peptide amphiphiles. (**c**) TEM (negative staining with 2% aqueous uranyl acetate) and (**d**) AFM of peptidic nanocarriers (**2a**) showing micellar aggregates (starting material). (**e**) AFM image of MMP-9 induced fiber formation (GFFAGL) (**2c**) after 96 h.

2.6. Confocal microscopy

Samples were imaged in a liquid state using a Nikon A1 (Tokyo, Japan), an Olympus FV1000 (Leica, Milton Keynes, UK) or a LSM 880 with Airyscan (Zeiss, Jena, Germany) at the Beatson Cancer Research Institute (Glasgow). Identical exposure times and processing were used in all experiments. Images were acquired using a 405 nm laser for DAPI, 488 nm laser for carboxyfluorescein, and 561 nm for phalloidin (Alexa^{568} labeled), over a field of view of 53 by 53 μm.

2.7. Cell culture, CRISPR and PMA stimulation

MDA-MB-231-luc-D3H2LN were cultured in Dulbecco's Modified Eagle Medium (DMEM) supplemented with 10% fetal bovine serum (FBS), 2 mmol/L L-glutamine and penicillin/streptomycin (100 units/mL and 100 μg/mL). Primers for sgRNAs sequences were designed for human MMP-9 (http://crispr.mit.edu/, see SM) and ligated into the BSMB1 cut vector lentiCRISPR [39]. Following lentiviral vector production with VSV and sPAX2 packaging plasmids in HEK-293T cells, MDA-MB-231-luc-D3H2LN cells were infected and subsequently selected using 1 μg/mL of puromycin.

For the stimulation of MMP-9 expression on glass/plastic with phorbol mristate acetate (PMA), cells were washed 3 times with PBS, serum starved and treated overnight with 100 nM of PMA.

2.8. Western blot and IHC analysis

The MMP-9 antibody (EP1255Y, Abcam) was used at a dilution of 1:1000 for Western blotting of cell culture extracts and 1:200 on fixed organotypic or subcutaneous tumor samples for immunohistochemistry (IHC). For Western blot analysis, cells were lysed using mRIPA buffer (50 mM Tris-HCl, 150 NaCl, 1% NP-40, 1% sodium deoxycholate, 0.1% SDS and 10 mM EDTA) supplemented with protease inhibitors aprotinin and leupeptin. After SDS-PAGE and transfer to a nitrocellulose membrane (Perkin Elmer), a chemiluminescence detection kit (Amersham) was employed in conjunction with the HRP-linked anti-rabbit IgG antibody (NEB 7074, Cell Signaling) at a 1:10,000 dilution to detect MMP-9 and GAPDH (2118, Cell Signaling) as a loading control. For IHC, standard processing and antigen-retrieval methods were applied using citrate buffer (pH = 6.0) and visualization and enhancement of the secondary biotinylated HRP-linked antibody was achieved by using the ABC Kit (Vectastain) and EnVision™ system (DAKO).

2.9. Zymography

Precast 10% zymogram (gelatin) protein gels (Novex™, ThermoFisher Scientific) were loaded with 20 μL of tissue culture medium, pre-spun at 1200 rpm for 5 min to remove cellular debris. Following SDS-PAGE, gels were renatured and developed in the respective buffers (Novex™) and finally developed for 24 h at 37 °C. Gels were then stained with SimplyBlue™ (ThermoFisher Scientific) and scanned.

2.10. Cytotoxicity assay

For MTT analysis of proliferation and cytotoxicity of the MMP-9 responsive peptides alone or in conjunction with doxorubicin (doxorubicin hydrochloride was used) on cells, 10^4 of MDA-MB-231-luc-D3H2LN cells were seeded per well in a 96 well plate format and allowed to settle overnight. The following day cells were washed 3 times with PBS and serum starved in serum free medium. They were then treated with 100 nM of PMA overnight and exposed to increasing concentrations of the respective peptides, doxorubicin alone or a combination of 2.5 mM of peptide plus increasing concentrations of doxorubicin for 72 h. Following drug exposure, 5 μL of MTT solution (5 mg/mL, Roche) was added per well and incubated to produce formazan for 3–4 h. Finally 100 μL of solubilization buffer (1:1 isopropanol:DMSO) was added, incubated overnight at 37 °C and the OD at 570 nm determined using a microplate reader (Safire 2, Tecan).

2.11. Organotypic culture matrices

Organotypic matrices and subsequent invasion assay was performed as described previously [40]. Briefly, 10^5 primary human fibroblasts, between the passages 4–8, were embedded in rat-tail extracted collagen. The detached polymerized mixture was allowed to contract into a malleable 3D matrix for up to 14 days in DMEM supplemented with 10% FBS and 2 mmol/L L-glutamine. 1×10^5 of MDA-MB-231-luc-D3H2LN were seeded on top of the matrices and left to settle for 24 h. They were then mounted unto a metal grid and an air-liquid-interface created allowing for the invasion process to start. After 3 days the medium below the grid was collected for the MMP-9 activity assay and the cultures fixed in 4% paraformaldehyde, followed by paraffin embedding and processing for haematoxylin and eosin staining. Blank sections were further stained with α-MMP9 antibody (EP1255Y, Abcam) for the visualization of MMP-9 expression in and around invading cells.

2.12. In vivo assessment of MMP-9 responsive peptides

2×10^6 cells were re-suspended after trypsinisation in 100 μL Hank's Balanced Salt Solution (HBSS, Invitrogen) and injected subcutaneously into the flanks of $CD1^{-/-}$ nude mice. Tumors were allowed to develop to a size of 280–400 mm^3 before the commencement of treatment. Animals were kept in a conventional animal facility and all experiments were carried out in compliance with the U.K. Home Office guidelines. Tumor bearing mice were treated with daily subcutaneous injections of either the vehicle 1:1 DMSO:PBS or a sub-clinically active dose of doxorubicin 1 mg/kg alone or in conjunction with the respective peptides at a concentration of 36 mg/kg. The tumor sizes were monitored every second day by caliper measurements and the tumor volume calculated using the ellipsoid formula [41].

2.13. MMP-9 activity assay

The activity of the MMP-9 was assessed using the SensoLyte® Plus 520 MMP-9 assay kit (Anaspec, Fremont, CA). Briefly, cell culture supernatants were collected after overnight serum exposure, serum starvation followed by stimulation with 100 nM PMA and 3 day invasion into organotypic matrices and centrifuged for 10 min at 1000× *g*, 4 °C. A black 96-well plate covered with MMP-9 antibodies was subsequently used to capture the (pro-)MMP-9 from the sample supernatant. An activation step with APMA (2 h) was performed in order to activate pro-MMP-9 and record a total signal of potential MMP-9 activity. After activation the assay substrate (5-FAM/QXL™ 520 FRET) was added and the fluorescence reading performed using a X-Fluor Safire 2 fluorescence plate reader ($\lambda_{ex}/\lambda_{em}$ 490 nm/520 nm). The amount of MMP-9 in each sample was calculated according to the manufacturers instruction on the basis of a standard curve of the catalytic responsive enzyme. The assay was performed in 3 independent experiments for each condition.

2.14. Inverted invasion assay

Transwell inserts with a pore size of 0.8 μm were used as described previously in an inverted invasion assay [42]. To that end, Matrigel (BD) was diluted with PBS to a concentration of 5 mg/mL and allowed to polymerize in the transwell at 37 °C for 30 min. Following this, MDA-MB-231-luc-D3H2LN cells expressing a GFP construct were seeded at a density of 5×10^4 cells on the inverted insert, directly on the porous membrane. Cells were allowed to adhere for up to 4 h and inserts placed upright into 24 well plates containing serum free medium alone or in combination with the peptides **1a**, **2a** and the respective D-peptide versions. DMEM plus 10% FBS and supplemented with 25 ng/mL EGF was added atop the Matrigel, establishing a FBS + EGF gradient across the Matrigel and cells allowed to invade for up to 5 days. Confocal microscopy was used to visualize the cells that crossed through the porous filter and optical sections acquired in 15 μm steps. For this, an inverted confocal microscope (Fluoview FV1000, Olympus) equipped with the acquisition software FV10-ASW1.7 was used. The measured fluorescent intensity was subsequently used to quantify the percentage of invading cells/relative invasion index past 30 μm into the Matrigel versus the total fluorescence intensity in all sections utilizing the ImageJ plugin Area Calculator.

3. Results and discussion

3.1. MMP-9 triggered micelle to fiber transition for entrapment of doxorubicin

Recent examples demonstrate the integration of enzymatic activity and molecular self-assembly (biocatalytic self-assembly) for the development of cancer therapy [22,35,38]. Typically, the molecular design of these structures involve hydrophobic (naphthalene, fluroenyl, lipidic) or polymeric moieties. We aimed to design a system that does not contain new chemical entities, focusing on alpha peptides, because of their inherent biocompatibility and biodegradability through proteolytic digestion to alpha amino acids. Thus, we designed peptide micelles for drug encapsulation, which reconfigure to less mobile fibrillar structures with selective tumor retention due to localized MMP-9 activity (Fig. 1a).

The design of the peptide sequence is based on MMP-9 triggered gelation reported by Xu and co-workers [27] and our previous work on MMP-9 induced micelle-to-fiber transitions of PhAc-FFAGLDD (**1a**) [43]. In addition, a peptidic GFFLGLDD analogue was designed (**2a**, not containing the phenylacetyl moiety) containing the fiber forming (GFFL/G) unit, the expected MMP-9 cleavable bond (G↓L) and the reconfiguration (DD) unit. For this design, the MEROPS database [44] was consulted, where the self-assembling units are incorporated into the MMP-9 substrate.

Peptides **1a/b** and **2a/b/c** were synthesized and characterized for self-assembly behavior (for HPLC and mass spectroscopy details see Figs. S1–S3). The characterization of peptide **1a** and **1b** alongside with the MMP-9 digestion of **1a** was previously reported [43]. The enzymatic cleavage of **2a** was assessed by treatment with MMP-9 at a concentration of 50 ng/mL [45,46], which is in the range of the MMP-9 concentration secreted by cancer cells determined in our experiments (see below). The conversion and product identification were assessed by HPLC and LCMS (Figs. S7 and S8). The near-complete enzymatic digestion of GFFLGLDD occurs between 48 and 96 h. Peptide **2a** shows conversion to a range of products, the main one being GFFLGL (**2c**), corresponding to the fragment that is one residue longer than the expected product, as previously observed with **1a** [43], indicating a shift in MMP-9 specificity (Fig. 1b) [47]. Other products that formed, but in lower quantities are GFF (+LGLDD) and (GF) + FLGLDD (Figs. S7 and S8). These results show that there is some residual cleavage by MMP-9 at the F↓L and F↓F bonds and is in accordance with previously observed ability of MMP-9 to cleave amyloid peptides [27,48,49]. As expected for amphiphilic compounds, AFM and TEM characterization of the precursors revealed spherical aggregates for **2a** (Fig. 1c and d). In contrast, chemically synthesized positive controls for compounds **2b** (Fig. S4a) and **2c** (Fig. S5a), produced fibrillar nanostructures. The morphological change induced by enzymatic cleavage was then monitored by AFM and TEM, confirming that upon enzymatic hydrolysis the micelles reconfigured into fibers, which were similar to those formed by the chemically synthesized cleavage products alone (Fig. 1e and Fig. S9). Thus, peptide **2a** is capable of undergoing MMP-9 triggered morphological micelle-to-fiber transition (Fig. 1c, d, 1e and Fig. S 9b), as reported previously for **1a** (also shown in Fig. S9a) [43].

The differential supramolecular organization underpinning this shape change was investigated by infrared (IR) spectroscopy (Figs. S4b and S5b), which suggested the presence of ordered structures [50]. Peptide **2a** shows a red shift (broad peak at 1643 cm^{-1}) compared to absorption values typical for free peptides in solution (1650–1655 cm^{-1}). The 1570–1580 cm^{-1} absorption band is attributed to the aspartic acid side chain carboxylate group present in **2a**. Extended structures are observed for **2b** (1630 cm^{-1}) showing a complex pattern [51]. β-sheet like structures were found for **2c** indicated by the presence of 1625 cm^{-1} peak (Fig. S5b).

Having established that the peptides were capable of undergoing a morphological change in response to MMP-9 activity, we next investigated whether a therapeutic drug could be encapsulated within the nanostructures. For this purpose, doxorubicin was solubilized in DMSO by sonication and a 1 mM stock solution in PBS was made and subsequently diluted into the suspension of peptide micelles (final concentration of doxorubicin: 5 μM). First, the effect of doxorubicin incorporation on the biocatalytic micelle-to-fiber conversion was investigated. To this end, the starting material (**2a**) and the observed product of MMP-9 cleavage (**2c**) were characterized by AFM and TEM in the presence of 0.2% of doxorubicin, to assess whether the micelle or fiber formation was disrupted by the presence of the drug. In the presence of doxorubicin, spherical aggregates are still observed for **2a** (Fig. S6a and S6b), and fibers for **2c** (Fig. S6d and S6e), Doxorubicin fluorescence was also imaged to assess whether the drug was incorporated in the nanostructures. Fluorescence signal (Fig. S6c and S6f) from doxorubicin emission is observed in both **2a** and **2c**, confirming its incorporation in peptide nanostructures. Confocal microscopy (Fig. S10b) confirms doxorubicin entrapment in the fibres after enzyme treatment, which is further confirmed by fluorescence studies (Fig. S10a), where a two-stage discontinuous behavior is shown upon treatment of peptide micelles with MMP-9. Due to difficulties in separating peptide fragments and doxorubicin, it was not possible to quantitatively determine the doxorubicin loading in the peptide nanostructures.

3.2. Treatment with MMP-9 responsive peptides combined with doxorubicin in vitro

Supramolecular peptide based systems have recently been shown to be successful for *in vitro* and *in vivo* inhibition of tumor progression based on polymeric nanocarriers (micellar peptide/polymer drug conjugates) [20] or formation of hydrophobic (NapFF), cytotoxic fibres [52]. Our approach differs in that we use peptidic nanocarriers to locally assemble into non-toxic nanostructured depots. To measure the response of the MDA-MB-231-luc-D3H2LN cells to the peptide micelles *in vitro*, cells had to first be serum starved in order to avoid the effect of non-specific cleavage by MMP-like enzymes contained in serum [53,54]. They were subsequently stimulated with 100 nM of PMA (Phorbol 12-myristate 13-acetate) in order to express MMP-9, which is secreted by cancer cells to promote 3D invasion [55] (Fig. 2a). Zymograms of the gelatinolytic properties of cell culture supernatants from the cancer cells showed the presence of several MMPs in the serum sample (with bands at around 90 and 70 kDa as expected for MMP-9 and MMP-2 respectively). Serum starved cells treated with PMA, however, only displayed a single degradation band at ~90 kDa, the expected size of MMP-9 (Fig. 2b). Specific MMP-9 cleavage activity was assessed by the use of a fluorimetric ELISA, showing that after PMA stimulation 18.5 ± 4.1 ng/mL of active enzyme could be detected (Fig. 2c).

Biocompatibility of MMP-9 cleavable peptides was then measured in cancer cells by the use of MTT assays. In addition, the non-cleavable D-stereoisomer analogues PhAc-^{D}F^{D}F^{D}AG^{D}LDD (**1a(D)**) and G^{D}F^{D}F^{D}LG^{D}LDD (**2a(D)**) were synthesized (Figs. S11 and S12) for comparison with the L-stereoisomers. The D-stereoisomers treated with MMP-9 showed no degradation for at least 10 days of treatment (Figs. S13 and S14). MTT assay showed no reduction in viability, while instead a slight increase in proliferation for **1a**, **1a(D)** and **2a(D)** (Fig. 2d, >100%). A minor reduction of cell viability for **2a** (Fig. 2d and 78.3 ± 14.5%) was observed at concentrations above the critical aggregation concentration of 2.5 mM.

When cells were treated with 2.5 mM of peptide micelles in conjunction with increasing concentrations of doxorubicin, an

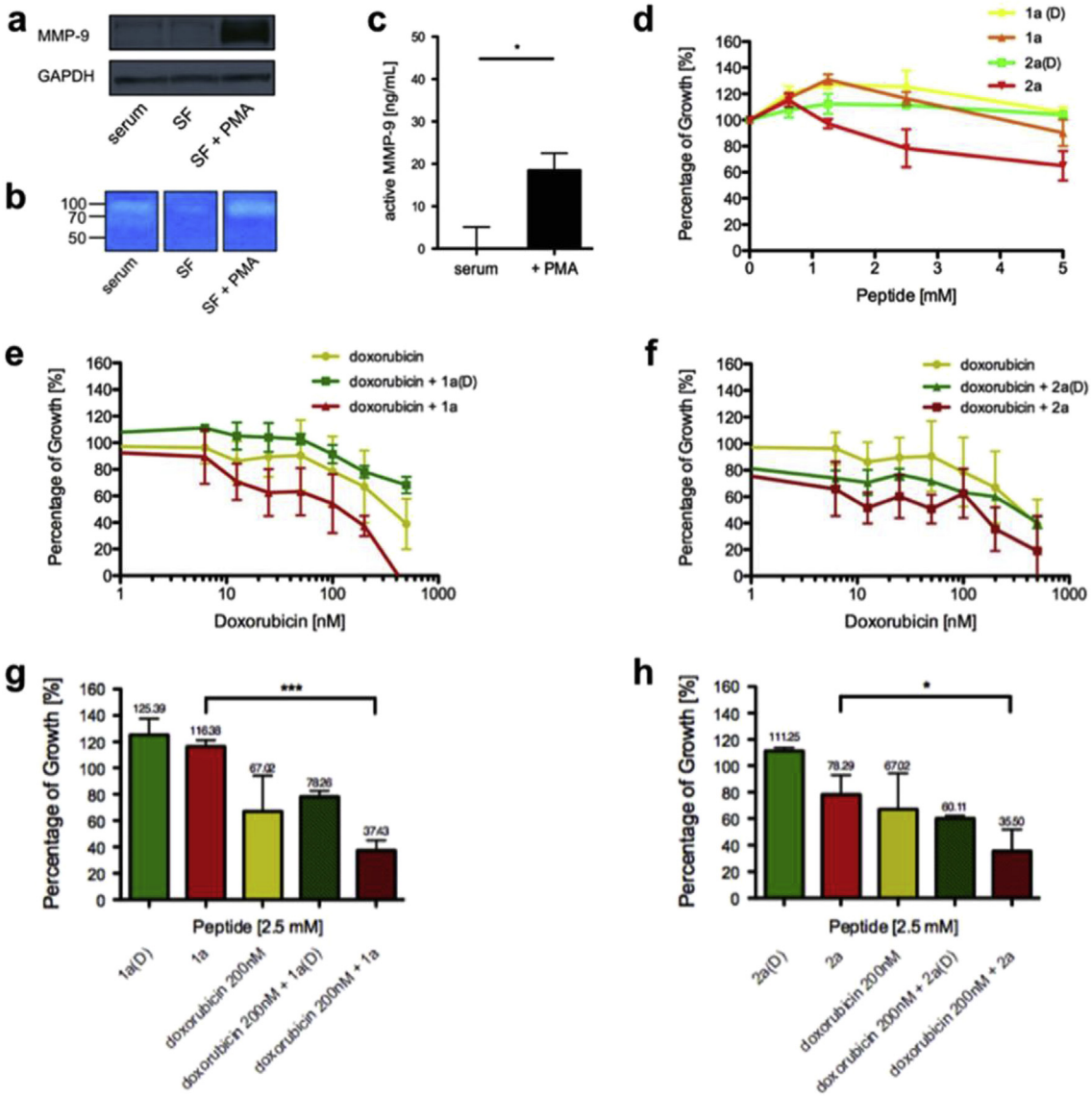

Fig. 2. Effect of MMP-9 cleavable peptides and doxorubicin on proliferation of cells *in vitro*. (**a**) MMP-9 expression in MDA-MB-231-luc-D3H2LN cells after serum starvation (SF) and stimulation with PMA (100 nM). (**b**) Zymogram of the gelatinolytic activity of cell culture supernatants of MDA-MB-231-D3H2LN cells before and after serum starvation (SF) ± 100 nM of PMA. (**c**) Specific MMP-9 activity was quantified for MDA-MB-231-luc-D3H2LN cells in serum and when cells were stimulated with 100 nM of PMA, by fluorimetric ELISA (bars: mean; error bars: SEM; $^{*}p < 0.05$ by standard student's *t*-test; n = 3 independent experiments). (**d**) MTT assay of MDA-MB-231-luc-D3H2LN cells after serum starvation (SF) and stimulation with PMA (100 nM) exposed to increasing concentrations of MMP-9 cleavable peptides **1a**, **2a** and their D-peptide versions after 3 days of incubation. (**e**) + (**f**) Combination treatment of cells with peptides **1a** and **2a** with doxorubicin at 2.5 mM of the respective peptide and histogram overview of results obtained at 2.5 mM peptides ± 200 nM doxorubicin (**g**) + (**h**), measured by MTT assay after 3 days (bars/dots: mean; error bars: SEM; $^{*}p < 0.05$, $^{***}p < 0.001$ by standard student's *t*-test; n = 3 independent experiments).

increased toxicity was observed especially for the MMP-9 cleavable peptides **1a** and **2a** (Fig. 2e–h). Critically, this behavior was not observed for the D-stereoisomers of the peptides, **1a(D)** and **2a(D)**, that are not susceptible to MMP-9 digestion (Figs. S13 and S14), therefore the micelle-to-fibre transition does not occur. In Fig. 2e–h the observed 60%–70% of viability in the doxorubicin treated samples is preserved in the combination treatments of D-peptide with doxorubicin. In the case of the L-peptide and doxorubicin combination the cell viability is drastically reduced to 37.5% and 35% for **1a** and **2a**, respectively.

Up to 5 mM peptide concentrations, both peptide micelle types **1a**/**2a** were found to have minimal effects on cell viability in the absence of doxorubicin (Fig. 2d). However, both peptides showed to increase the effectiveness of doxorubicin over a wide range of concentrations (6.25–500 nM) (Fig. 2e and f). In contrast, neither of the non-hydrolysable D-stereoisomers showed this amplification of the effects of doxorubicin treatment. **1a(D)** even reduced the effectiveness of doxorubicin treatment, consistent with the idea that doxorubicin could be trapped by peptide micelles, but not released through enzymatic cleavage. Thus, the combination treatment was more toxic to cancer cells compared to doxorubicin alone and also compared to the combination of the D-peptides and doxorubicin, confirming the crucial role of MMP-9 in micelle-mediated drug delivery. These data support a mechanism, whereby the micelle-to-fibre morphology transition results in increased toxicity of the combination treatment due to the formation of fibrillar depots which act to localize the drug near the cancer cells.

3.3. Visualization of peptide nanostructures in vitro

Imaging exogenous peptide nanostructures in the proximity of cells was challenging, mainly because of the lack of intrinsic fluorescence of the peptide assemblies. Signal visualization by confocal microscopy was achieved by co-assembling small percentage (1%) of fluorescently tagged peptide-conjugates with micelle forming peptides [56,57]. To this end, peptide **2a** was labeled with carboxyfluorescein. Carboxyfluorescein-**2a** ($\lambda_{ex/em}$ = 492/517 nm) and **2a** co-assemblies were prepared by mixing the two molecules at a ratio of 1/100, followed by sonication. They were imaged using AFM, TEM and fluorescence microscopy (Fig. S15). These results show that the carboxyfluorescein-**2a** and **2a** co-assemble into spherical aggregates and that carboxyfluorescein is incorporated in the micelles, which made it a good candidate for imaging the distribution of peptides after administration to cells (Fig. 3a).

The imaging of peptides, by laser-scanning confocal microscopy with subsequent deconvolution using an Airyscan unit (Zeiss), in proximity to cancer cells *in vitro* shows that the peptidic carriers are found in the cytoplasm and nuclei of the cancer cells (pink arrows) with some larger aggregates (orange arrows) also detected outside the cells. The formation of fibrillar nanostructures becomes apparent in the larger aggregates outside of the cell which was further confirmed by SEM (Fig. 3b).

Resolution limitations of confocal microscopy make it difficult to be conclusive on peptide morphology (micelles or fibres) in proximity to cancer cells. However, signal detection is useful for confirmation of the peptides positioning in proximity of cancer cells. Moreover, substantial peptide uptake can be noticed (Fig. 3a,

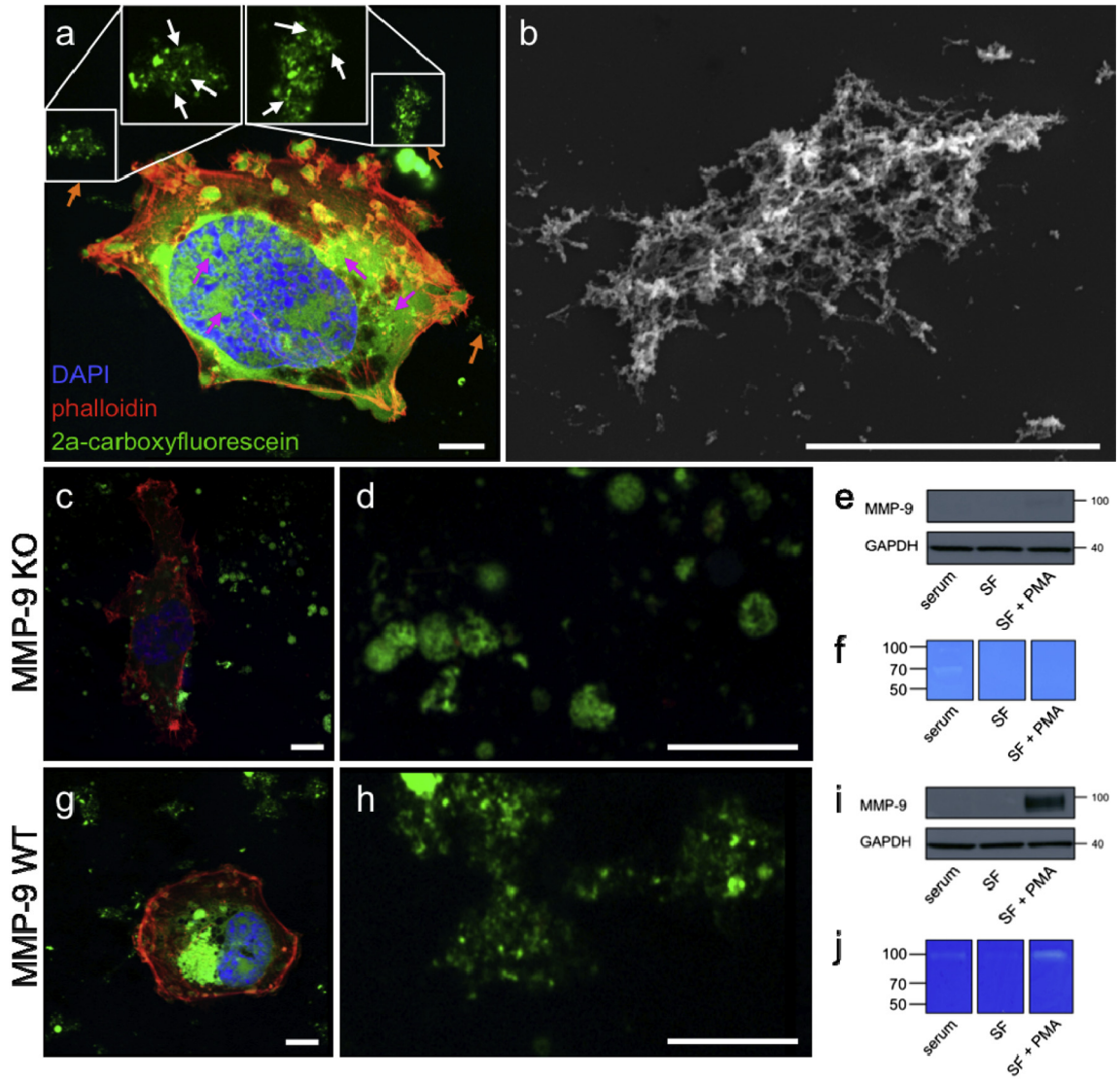

Fig. 3. Imaging of peptides in proximity of cancer cells *in vitro*, with loss of aggregate fibrillar morphology observed upon MMP-9 knockout. (**a**) 2D Airyscan captured representative image of MDA-MB-231-luc-D3H2LN breast cancer cells cultured for 3 days in the presence of **2a** + **2a**-carboxyfluorescein (green) and 100 nM PMA, inducing MMP-9 expression. The actin cytoskeleton was stained with phalloidin-Alexa^{568} (red) and the nuclei with DAPI (blue). Extra-cellular peptidic aggregates were further magnified and fibrillar features highlighted (white arrows). Spherical bodies of the peptidic carrier were detected in and around the cancer cells as well as fibrillar aggregates formed (orange arrows); with accumulation of the peptides in the cytoplasm and nuclei of cells (pink arrows); (**b**) Extracellular aggregates of peptide **2a** visualized by SEM; (**c**) + (**g**) Airyscan captured representative images of peptidic structures around MDA-MB-231-luc-D3H2LN MMP-9 KO and WT cells treated and stained as in (**a**); Extra-cellular peptidic aggregates were further magnified (**d**) + (**h**); representative immunoblots shown for MMP-9 expression for both KO and WT cells (**e**) + (**i**) as well as zymograms of the gelatinolytic activity of cell culture supernatants after serum starvation (SF) and stimulation with PMA (100 nM) (**f**) + (**j**); scale bars: 5 μm.

g). Furthermore, the genetic editing and deletion of MMP-9 expression using CRIPSR-Cas9 technology, goes on to demonstrate the need of MMP-9 presence around the cells in order for spherical, micellar aggregates to be efficiently converted into fibrillar network-like nanostructures (see Fig. 3c and d versus 3 g and 3 h).

3.4. Treatment with MMP-9 responsive peptides augments doxorubicin toxicity in vivo

After showing the synergistic effect of peptide amphiphiles loaded with doxorubicin *in vitro* and demonstrating formation of fibrillar aggregates in proximity of MMP-9 secreting cells, we moved on to investigate whether the doxorubicin loaded peptide carriers could increase the effectiveness of doxorubicin *in vivo*. First, an *in vivo* imaging dye to visualize MMPs, MMPSense680™, was injected intravenously and imaged 2 h after injection in MDA-MB-231-luc-D3H2LN developed xenograft tumors, revealing high MMP activity at the primary tumor site (Fig. 4a). MMP-9 expression has been demonstrated in primary human breast cancer tumors samples before by IHC (Immunohistochemistry) [58]. Here, the presence of MMP-9 was also visualized by IHC in the developed xenograft tumors and found to be increased at the invasive border of the subcutaneous tumors (Fig. 4b). In order to assess the effect of MMP-9 cleavable peptidic carriers on the delivery and the effect of sub-clinically administered doses of chemotherapeutics, nude mice were allowed to develop primary tumors of a size between 280 and 400 mm^3. They were then grouped randomly into treatment groups of 3–4 mice, receiving daily subcutaneous (s.c.) injections, distal to the primary tumor site, of either the

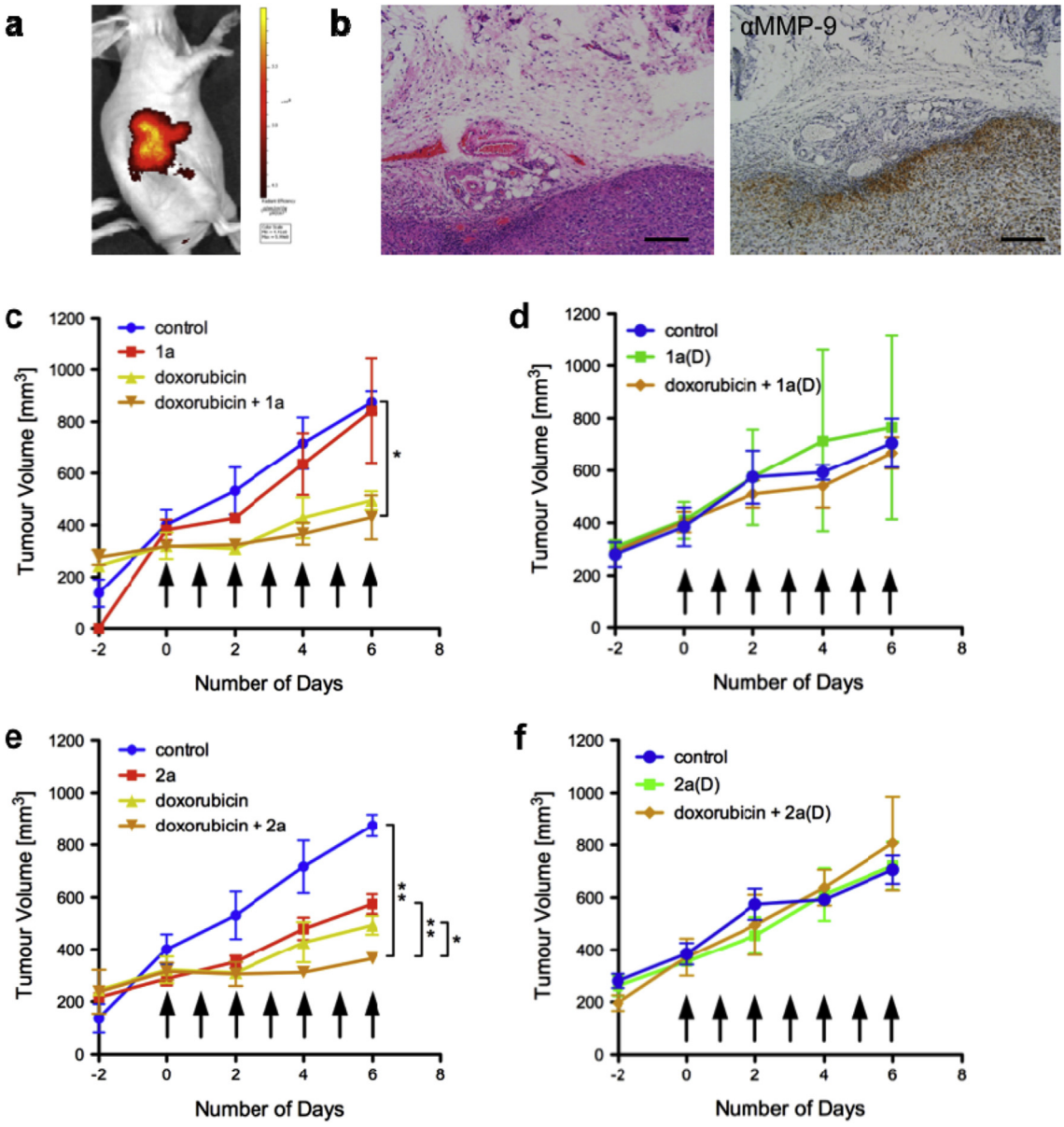

Fig. 4. MMP-9 cleavable peptide carriers augment doxorubicin treatment *in vivo*. (**a**) MMPSense680™ reporting on MMP activity *in vivo* in a subcutaneous tumor of MDA-MB-231-luc-D3H2LN. (**b**) Representative H&E and IHC of human MMP-9 expression at the invasive border of a MDA-MB-231-luc-D3H2LN subcutaneous xenograft tumor; scale bars: 100 μm. (**c**) + (**e**) *In vivo* tumor progression of MDA-MB-231-luc-D3H2LN subcutaneous tumors treated with **1a** (**c**) or **2a** (**e**) (36 mg/kg), doxorubicin at a low concentration (1 mg/kg) or in combination of the two, by s.c. injection, showing stasis of tumor growth in the combination treatment. (**d**) + (**f**) Treatment with D-peptides did not result in an additive effect (arrows: time points of treatment; data point: mean; error bars: SEM; n = 3–4 mice per treatment group; *p < 0.05 and **p < 0.01 by standard student's *t*-test).

control (1:1 PBS:DMSO), a sub-clinically effective dose of doxorubicin (1 mg/kg) [59,60], the respective peptide carrier (36 mg/kg), or a combination of the two. This revealed that the MMP-9 cleavable peptide carriers **1a** and **2a** augment doxorubicin toxicity when administered in tandem. When compared to the doxorubicin only treatment cohort, the peptide carrier/doxorubicin treatment, especially with **2a**, shows to render the tumors in a static progression (Fig. 4c and e). Furthermore, the treatment with only **1a** had no effect on tumor progression, while **2a** seemed to have some delaying effect on tumor growth. This differential effect on tumor growth is in agreement with *in vitro* results showing reduced cell growth in the presence of **2a** (Fig. 2g/h). On the other hand, the D-peptide versions of both, **1a(D)** and **2a(D)**, as well as their combination with doxorubicin, had no effect on tumor progression (Fig. 4d and f). In fact the combination of the D-peptide with the doxorubicin seems to hamper the effect of the chemotherapeutic, compared to when solely doxorubicin was administered, suggesting doxorubicin is not effectively released from the micellar precursors. This demonstrates that MMP-9 cleavable peptide carriers in conjunction with doxorubicin have an increased effect on toxicity toward the developed tumor mass. In addition to the tumor site specific cleavage of the peptide micelles and the local release of the chemotherapeutic, the observed increased toxicity of the combination treatment could be attributed to the possibility of forming reservoirs of doxorubicin at the MMP-9 rich tumor site, with the cleaved peptidic carrier incorporating doxorubicin when forming fibers, as observed *in vitro*.

3.5. Invasion of MDA-MB-231-luc-D3H2LN is significantly decreased in the presence of MMP-9 responsive peptide carriers

MMP-9 has previously been found to be up-regulated and associated with invasiveness of the breast cancer cell line MDA-MB-231 [61–63]. Expression of, for example α3β1 integrin, on invading MDA-MB-231 cells has been found to be a key regulator in the expression of MMP-9 during invasion of these cancer cells [61].

Indeed here, MMP-9 expression was detected in organotypic matrices, a 3D invasion model, by IHC, after MDA-MB-231-luc-D3H2LN cells had invaded for up to 5 days into the collagen matrix (Fig. 5a). Further, the activity of specifically MMP-9 in the culture medium of the organotypic matrices was measured by fluorimetric ELISA, following three days of invasion of the MDA-MB-231-luc-D3H2LN cells (Fig. 5b). Notably, MMP-9 expression has previously been found to be particularly stimulated when MDA-MB-231 cells came in contact with extracellular matrix components and especially matrigel *in vitro*, potentially aiding invasion [62]. Due to the fact that we observed increased MMP-9 expression at the invasive edge of the subcutaneous tumors (see Fig. 4b), we wanted to assess whether the peptides themselves had any effect on the invasion of cells. In order to assess the effect on invasion of the MMP-9 cleavable peptidic carriers alone, MDA-MB-231-luc-D3H2LN cells were allowed to invade in an inverse invasion assay, containing matrigel, for up to 5 days (Fig. 5c) [42]. Cells exposed to 2.5 mM of either peptide **1a** or **2a** showed a significant reduction in their invasion (Fig. 5d). Scanning Electron Microscopy (SEM) further

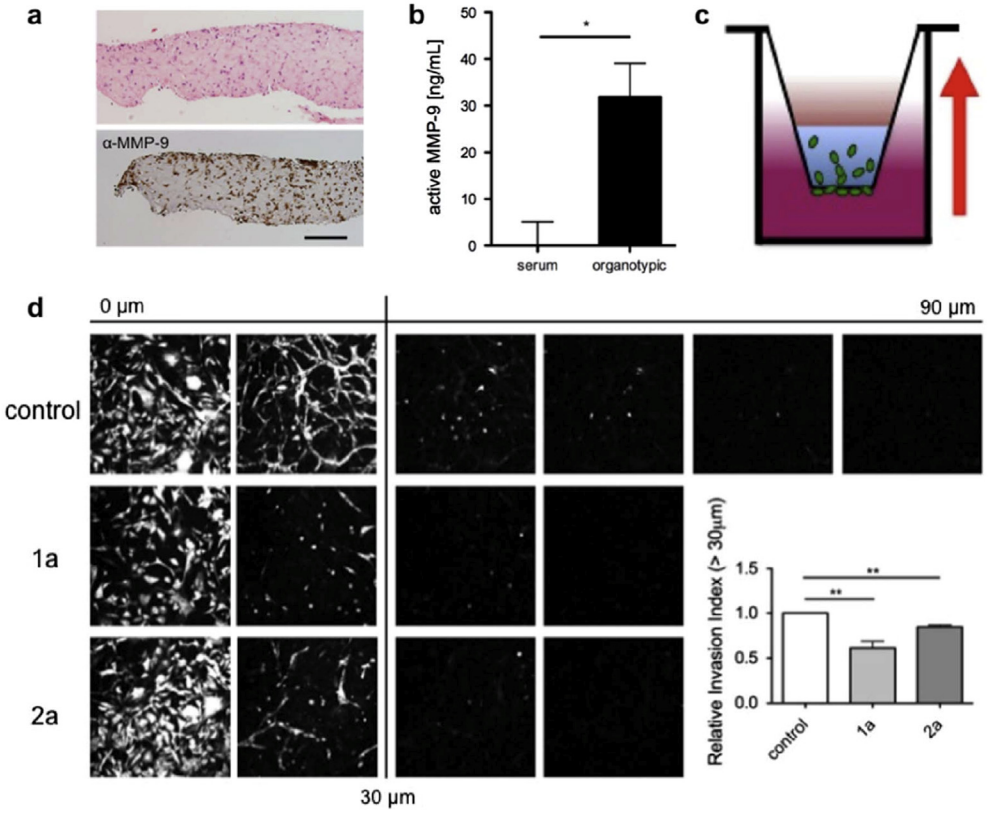

Fig. 5. The effect of MMP-9 cleavable peptides on the invasion of cells. (**a**) IHC of MMP-9 of invading MDA-MB-231-luc-D3H2LN on an organotypic matrix; scale bars 100 µm. (**b**) MMP-9 activity was quantified for MDA-MB-231-luc-D3H2LN in serum and when cells are seeded on an organotypic matrix, by fluorimetric ELISA (bars: mean; error bars: SEM; $^{*}p < 0.05$ by standard student's *t*-test; n = 3 independent experiments). (**c**) Schematic of an inverted invasion assay set-up, with the GFP expressing cells (green) on the bottom of the insert in serum free medium (pink), migrating toward a serum and EGF gradient (serum + EGF containing medium in brown) into the matrigel (blue). (**d**) Inverse invasion assay of MDA-MB-231-luc-D3H2LN expressing a GFP construct, invading into matrigel, with 0 µm denoting cells that have gone through the filter but not into the gel, quantified by measuring the fluorescence intensity of cells penetrating above 30 µm (bars: mean; error bars: SEM; $^{**}p < 0.01$ by standard student's *t*-test; n = 3 independent experiments). (For interpretation of the references to colour in this figure legend, the reader is referred to the web version of this article.)

showed an alteration in the lamellipodia formation of the cells stimulated with PMA and treated with the L-peptide **2a**, but not the D-peptide **2a**, indicating possible hindrance of migration (Fig. S16). Further, the quantification of circulating tumor cells (CTCs) in the blood of the xenograft mice was performed. CTCs have an important role as markers of tumor progression and as such could be applied to reveal drug resistance in real time [64]. Here, we observed a rescue effect of combination treatment of doxorubicin and **2a** compared to the elevated number of CTCs measured for doxorubicin treatment alone (Fig. S17). Having shown that MMP-9 expression is particularly prominent at the tumor border of xenograft subcutaneous MDA-MB-231-luc-D3H2LN tumors, the treatment with these peptidic carriers could localize drug delivery and retentions at these crucial sites of tumor progression. The additional effect of the treatment with the peptides alone hindering invasion in a 3D *in vitro* assay could be another benefit of treating the primary tumor with the peptidic carrier, potentially hampering metastatic dissemination.

4. Conclusions

In summary, peptides may act as 'safe' and highly tuneable building blocks of nanostructures, which are attractive due to low toxicity of their degradation products. Therefore, peptides and polymer-peptide conjugates gained attention in the last two decades as designable alternatives to liposomal nanostructures that have reached the clinic as doxorubicin vehicles for cancer treatment (example Doxil). More recently, nanoscale peptide vectors used for physical encapsulation of anticancer drugs were able to show better performance compared to the drugs only [38,65,66]. Here, two different MMP-9 responsive peptide amphiphiles able to self-assemble into spherical aggregates that undergo enzyme triggered micelle to fiber transition and are capable of encapsulation and controlled release of doxorubicin are presented. These mobile carriers of anticancer drugs are designed to selectively deliver the payload to tumor tissues, where they assemble to form localized fibrous depots by exploiting invasive border associated MMP-9 overexpression. The assembled fibers provide a depot for prolonged drug delivery due to partial entrapment of the drug and the intrinsic biodegradable nature of peptide carriers themselves. Unlike previously reported peptide conjugates, these systems have the advantage of being non-toxic to cells (as shown by MTT assay) and can be used as carriers for doxorubicin *in vivo*. When tested on xenograft tumor models, the cancer growth was halted by administration of doxorubicin loaded peptide nanostructures. In contrast to the combination therapies, where the peptide on its own has a toxic effect, here, the peptides themselves are non-toxic and are used as nanocarriers that can enhance the effectiveness of doxorubicin, trapped within the peptide nanostructure. This approach opens up the possibility of developing new (enzyme responsive) drug delivery vehicles designed to release drug payload locally, in the presence of the desired enzyme with potential application in cancer therapy.

Acknowledgements

The authors would like to acknowledge the Tong Wang at the Imaging Facility of CUNY Advanced Science Research Center for instrument use (TEM), scientific and technical assistance; Patricia Keating at the University of Strathclyde Mass Spectrometry facility for the help and support with analytical techniques and for valuable discussions; Margaret Mullin at the University of Glasgow for SEM and Margaret O'Prey at the CRUK Beatson Institute for help on the Zeiss LSM 880 Airyscan. We gratefully acknowledge EPSRC and Cancer Research UK for funding.

Appendix A. Supplementary data

Supplementary data related to this article can be found at http://dx.doi.org/10.1016/j.biomaterials.2016.04.039.

References

[1] C.L. Ventola, The nanomedicine revolution: part 1: emerging concepts, Pharm. Ther. 37 (2012) 512–525.
[2] D.J. Bharali, S.A. Mousa, Emerging nanomedicines for early cancer detection and improved treatment: current perspective and future promise, Pharmacol. Ther. 128 (2010) 324–335.
[3] C.G. Da Silva, F. Rueda, C.W. Löwik, F. Ossendorp, L.J. Cruz, Combinatorial prospects of nano-targeted chemoimmunotherapy, Biomaterials 83 (2016) 308–320.
[4] A. Schroeder, et al., Treating metastatic cancer with nanotechnology, Nat. Rev. Cancer 12 (2011) 39–50.
[5] T. Safra, et al., Pegylated liposomal doxorubicin (doxil): reduced clinical cardiotoxicity in patients reaching or exceeding cumulative doses of 500 mg/m2, Ann. Oncol. (2000) 1029–1033.
[6] J.D. Patel, et al., Clinical cancer advances 2013: annual report on progress against cancer from the American society of clinical oncology, J. Clin. Oncol. 32 (2014) 129–160.
[7] E. Miele, G.P. Spinelli, E. Miele, F. Tomao, S. Tomao, Albumin-bound formulation of paclitaxel (Abraxane® ABI-007) in the treatment of breast cancer, Int. J. Nanomed. 4 (2009) 99–105.
[8] X. Wang, L. Yang, Z.G. Chen, D.M. Shin, Application of nanotechnology in cancer therapy and imaging, CA. Cancer J. Clin. 58 (2008) 97–110.
[9] E. a Appel, et al., Self-assembled hydrogels utilizing polymer–nanoparticle interactions, Nat. Commun. 6 (2015) 1–9.
[10] D.J. Smith, et al., A multiphase transitioning peptide hydrogel for suturing ultrasmall vessels, Nat. Nanotechnol. (2015), http://dx.doi.org/10.1038/nnano.2015.238.
[11] J. Bhattacharyya, et al., A paclitaxel-loaded recombinant polypeptide nanoparticle outperforms Abraxane in multiple murine cancer models, Nat. Commun. 6 (2015) 7939.
[12] C.J. Newcomb, et al., Cell death versus cell survival instructed by supramolecular cohesion of nanostructures, Nat. Commun. 5 (2014) 3321.
[13] L. Zhao, et al., A review of polypeptide-based polymersomes, Biomaterials 35 (2014) 1284–1301.
[14] S. Zhang, Fabrication of novel biomaterials through molecular self-assembly, Nat. Biotechnol. 21 (2003) 1171–1178.
[15] S. Zhang, X. Zhao, L. Spirio, PuraMatrix: self-assembling peptide nanofiber scaffolds, Scaffolding Tissue Eng. (2005) 217–238.
[16] Z.-H. Peng, J. Kopecek, Enhancing accumulation and penetration of HPMA copolymer doxorubicin conjugates in 2D and 3D prostate Cancer cells via iRGD conjugation with an MMP-2 cleavable spacer, J. Am. Chem. Soc. 137 (2015) 6726–6729.
[17] A. Barnard, D.K. Smith, Self-assembled multivalency: dynamic ligand arrays for high-affinity binding, Angew. Chem. Int. Ed. 51 (2012) 6572–6581.
[18] N. Li, et al., Amphiphilic peptide dendritic copolymer-doxorubicin nanoscale conjugate self-assembled to enzyme-responsive anti-cancer agent, Biomaterials 35 (2014) 9529–9545.
[19] M.E. Hahn, N.C. Gianneschi, Enzyme-directed assembly and manipulation of organic nanomaterials, Chem. Commun. 47 (2011) 11814.
[20] C.E. Callmann, et al., Therapeutic enzyme-responsive nanoparticles for targeted delivery and accumulation in tumors, Adv. Mater. 27 (2015) 4611–4615.
[21] A. Tanaka, et al., Cancer cell death induced by the intracellular self-assembly of an enzyme-responsive supramolecular gelator, J. Am. Chem. Soc. 137 (2015) 770–775.
[22] J. Zhou, B. Xu, Enzyme-instructed self-assembly: a multi-step process for potential Cancer therapy, Bioconjug. Chem. 26 (2015) 987–999.
[23] M.J. Webber, C.J. Newcomb, R. Bitton, S.I. Stupp, Switching of self-assembly in a peptide nanostructure with a specific enzyme, Soft Matter 7 (2011) 9665.
[24] M. Zelzer, S.J. Todd, A.R. Hirst, T.O. McDonald, R.V. Ulijn, Enzyme responsive materials: design strategies and future developments, Biomater. Sci. 1 (2013) 11–39.
[25] A. Noël, M. Jost, E. Maquoi, Matrix metalloproteinases at cancer tumor-host interface, Semin. Cell Dev. Biol. 19 (2008) 52–60.
[26] K. Kessenbrock, V. Plaks, Z. Werb, Matrix metalloproteinases: regulators of the tumor microenvironment, Cell 141 (2010) 52–67.
[27] Z. Yang, M. Ma, B. Xu, Using matrix metalloprotease-9 (MMP-9) to trigger supramolecular hydrogelation, Soft Matter 9 (2009) 2546–2548.
[28] M.P. Lutolf, G.P. Raeber, A.H. Zisch, N. Tirelli, J. a Hubbell, Cell-responsive synthetic hydrogels, Adv. Mater. 15 (2003) 888–892.
[29] P.K. Vemula, et al., On-demand drug delivery from self-assembled nanofibrous gels: a new approach for treatment of proteolytic disease, J. Biomed. Mater. Res. Part A 97A (2011) 103–110.
[30] T. Gajanayake, et al., A single localized dose of enzyme-responsive hydrogel improves long-term survival of a vascularized composite allograft, Sci. Transl. Med. 6 (2014), 249ra110.
[31] Y.-A. Lin, Y.-C. Ou, A.G. Cheetham, H. Cui, Rational design of MMP degradable

peptide-based supramolecular filaments, Biomacromolecules 15 (2014) 1419–1427.
[32] D. Koda, T. Maruyama, N. Minakuchi, K. Nakashima, M. Goto, Proteinase-mediated drastic morphological change of peptide-amphiphile to induce supramolecular hydrogelation, Chem. Commun. (Camb). 46 (2010) 979–981.
[33] S.C. Bremmer, A.J. McNeil, M.B. Soellner, Enzyme-triggered gelation: targeting proteases with internal cleavage sites, Chem. Commun. 50 (2014) 1691–1693.
[34] D. Bacinello, E. Garanger, D. Taton, K.C. Tam, S. Lecommandoux, Enzyme-degradable self-assembled nanostructures from polymer-peptide hybrids, Biomacromolecules 15 (2014) 1882–1888.
[35] Y. Kuang, et al., Pericellular hydrogel/nanonets inhibit Cancer cells, Angew. Chem. Int. Ed. 53 (2014) 8104–8107.
[36] R. a Pires, et al., Controlling Cancer cell fate using localized biocatalytic self-assembly of an aromatic carbohydrate amphiphile, J. Am. Chem. Soc. 137 (2015) 576–579.
[37] M.P. Chien, et al., Enzyme-directed assembly of a nanoparticle probe in tumor tissue, Adv. Mater. 25 (2013) 3599–3604.
[38] J. Li, et al., Enzyme-Instructed intracellular molecular self-assembly to boost activity of cisplatin against drug-resistant Ovarian Cancer cells, Angew. Chem. (2015), http://dx.doi.org/10.1002/ange.201507157.
[39] N.E. Sanjana, O. Shalem, F. Zhang, Improved vectors and genome-wide libraries for CRISPR screening, Nat. Methods 11 (2014) 006726.
[40] P. Timpson, et al., Organotypic collagen I assay: a malleable platform to assess cell behaviour in a 3-dimensional context, J. Vis. Exp. 56 (2011) e3089.
[41] M.M. Tomayko, C.P. Reynolds, Determination of subcutaneous tumor size in athymic (nude) mice, Cancer Chemother. Pharmacol. 24 (1989) 148–154.
[42] R.F. Hennigan, K.L. Hawker, B.W. Ozanne, Fos-transformation activates genes associated with invasion, Oncogene 9 (1994) 3591–3600.
[43] D. Kalafatovic, et al., MMP-9 triggered micelle-to-fibre transitions for slow release of doxorubicin, Biomater. Sci. 3 (2015) 246–249.
[44] N.D. Rawlings, A.J. Barrett, MEROPS: the peptidase database, Nucleic Acids Res. 27 (1999) 325–331.
[45] A. Dilly, et al., Platelet-type 12-lipoxygenase induces MMP9 expression and cellular invasion via activation of PI3K/Akt/NF-κB, Int. J. Cancer 133 (2013) 1784–1791.
[46] M.E. Hahn, L.M. Randolph, L. Adamiak, M.P. Thompson, N.C. Gianneschi, Polymerization of a peptide-based enzyme substrate, Chem. Commun. (Camb). 49 (2013) 2873–2875.
[47] Y. Huang, J. Shi, D. Yuan, N. Zhou, B. Xu, Length-dependent proteolytic cleavage of short oligopeptides catalyzed by matrix metalloprotease-9, Biopolymers 100 (2013) 790–795.
[48] M. Hernandez-Guillamon, et al., Sequential Abeta degradation by the matrix metalloproteases MMP-2 and MMP-9, J. Biol. Chem. 290 (2015) 15078–15091.
[49] J.R. Backstrom, G.P. Lim, M.J. Cullen, Z. a Tökés, Matrix metalloproteinase-9 (MMP-9) is synthesized in neurons of the human hippocampus and is capable of degrading the amyloid-beta peptide (1-40), J. Neurosci. 16 (1996) 7910–7919.
[50] S. Fleming, et al., Assessing the utility of infrared spectroscopy as a structural diagnostic tool for β-sheets in self-assembling aromatic peptide amphiphiles, Langmuir 29 (2013) 9510–9515.
[51] A. Barth, C. Zscherp, What vibrations tell us about proteins, Q. Rev. Biophys. 35 (2002) 369–430.
[52] Y. Kuang, X. Du, J. Zhou, B. Xu, Supramolecular nanofibrils inhibit Cancer progression in vitro and in vivo, Adv. Healthc. Mater. 3 (2014) 1217–1221.
[53] S.B. Somiari, et al., Circulating MMP2 and MMP9 in breast cancer – potential role in classification of patients into low risk, high risk, benign disease and breast cancer categories, Int. J. Cancer 119 (2006) 1403–1411.
[54] H. Frankowski, Y. Gu, J. Heo, R. Milner, G. del Zoppo, Use of gel zymography to examine matrix metalloproteinase (gelatinase) expression in brain tissue or in primary glial cultures, Astrocytes Methods Protoc. 814 (2012) 221–233.
[55] M. Björklund, E. Koivunen, Gelatinase-mediated migration and invasion of cancer cells, Biochim. Biophys. Acta 1755 (2005) 37–69.
[56] Y. Gao, J. Shi, D. Yuan, B. Xu, Imaging enzyme-triggered self-assembly of small molecules inside live cells, Nat. Commun. 3 (2012) 1033.
[57] Y. Gao, et al., Probing nanoscale self-assembly of nonfluorescent small molecules inside live mammalian cells, ACS Nano 7 (2013) 9055–9063.
[58] J. Jones, P. Glynn, R. Walker, Expression of MMP-2 and MMP-9, their inhibitors, and the activator MT1-MMP in primary breast carcinomas, J. Pathol. 168 (1999) 161–168.
[59] M. Richter, et al., Preclinical safety and efficacy studies with an affinity-enhanced epithelial junction opener and PEGylated liposomal doxorubicin, Mol. Ther. Methods Clin. Dev. (2015), http://dx.doi.org/10.1038/mtm.2015.5.
[60] B. Yoo, et al., Combining miR-10b-targeted nanotherapy with low-dose doxorubicin elicits durable regressions of metastatic breast Cancer, Cancer Res. 75 (2015) 4407–4415.
[61] M. Morini, et al., The α3β1 integrin is associated with mammary carcinoma cell metastasis, invasion, and gelatinase B (mmp-9) activity, Int. J. Cancer 87 (2000) 336–342.
[62] M. Balduyck, et al., Specific expression of matrix metalloproteinases 1, 3, 9 and 13 associated with invasiveness of breast cancer cells in vitro, Clin. Exp. Metastasis 18 (2000) 171–178.
[63] J. Lee, et al., A matrix metalloproteinase inhibitor, batimastat, retards the development of osteolytic bone metastases by MDA-MB-231 human breast cancer cells in Balb C nu/nu mice, Eur. J. Cancer 37 (2001) 106–113.
[64] B. Hong, Y. Zu, Detecting circulating tumor cells: current challenges and new trends, Theranostics 3 (2013) 377–394.
[65] J. Naskar, G. Palui, A. Banerjee, Tetrapeptide-based hydrogels: for encapsulation and slow release of an anticancer drug at physiological ph, J. Phys. Chem. B 113 (2009) 11787–11792.
[66] P. Zhang, A.G. Cheetham, Y. Lin, H. Cui, Self-assembled tat nano fibers as E ffective drug carrier and transporter, ACS Nano 7 (2013) 5965–5977.

Supplementary Information

MMP-9 triggered self-assembly of doxorubicin nanofiber depots halts tumor growth

Daniela Kalafatovic[a†]*, *Max Nobis*[b†], *Jiye Son*[a,e], *Kurt I. Anderson*[b,f]* and *Rein V. Ulijn*[a,c,d,e]*

[a] Advanced Science Research Center (ASRC), City University New York, 85 St Nicholas Terrace, New York, NY 10031 (USA).

[b] CRUK Beatson Institute, Garscube Estate, Glasgow, G61 1BD (UK)

[c] WestCHEM, Department of Pure and Applied Chemistry, University of Strathclyde, 295 Cathedral Street, Glasgow G1 1XL (UK)

[d] Department of Chemistry and Biochemistry, City University of New York – Hunter College, 695 Park Ave., New York, NY 10065 (USA)

[e] Ph.D. Program in Chemistry, The Graduate Center of the City University of New York, New York, NY 10016 (USA)

[f] The Francis Crick Institute, 215 Euston Road, London NW1 2BE (UK)

* To whom the correspondence should be addressed:

Prof. Dr. Rein V. Ulijn, email: Rein.Ulijn@asrc.cuny.edu;

Dr. Daniela Kalafatovic, email: daniela.kalafatovic@irbbarcelona.org

Prof. Dr. Kurt Anderson, email: kurt.anderson@crick.ac.uk

† These authors contributed equally.

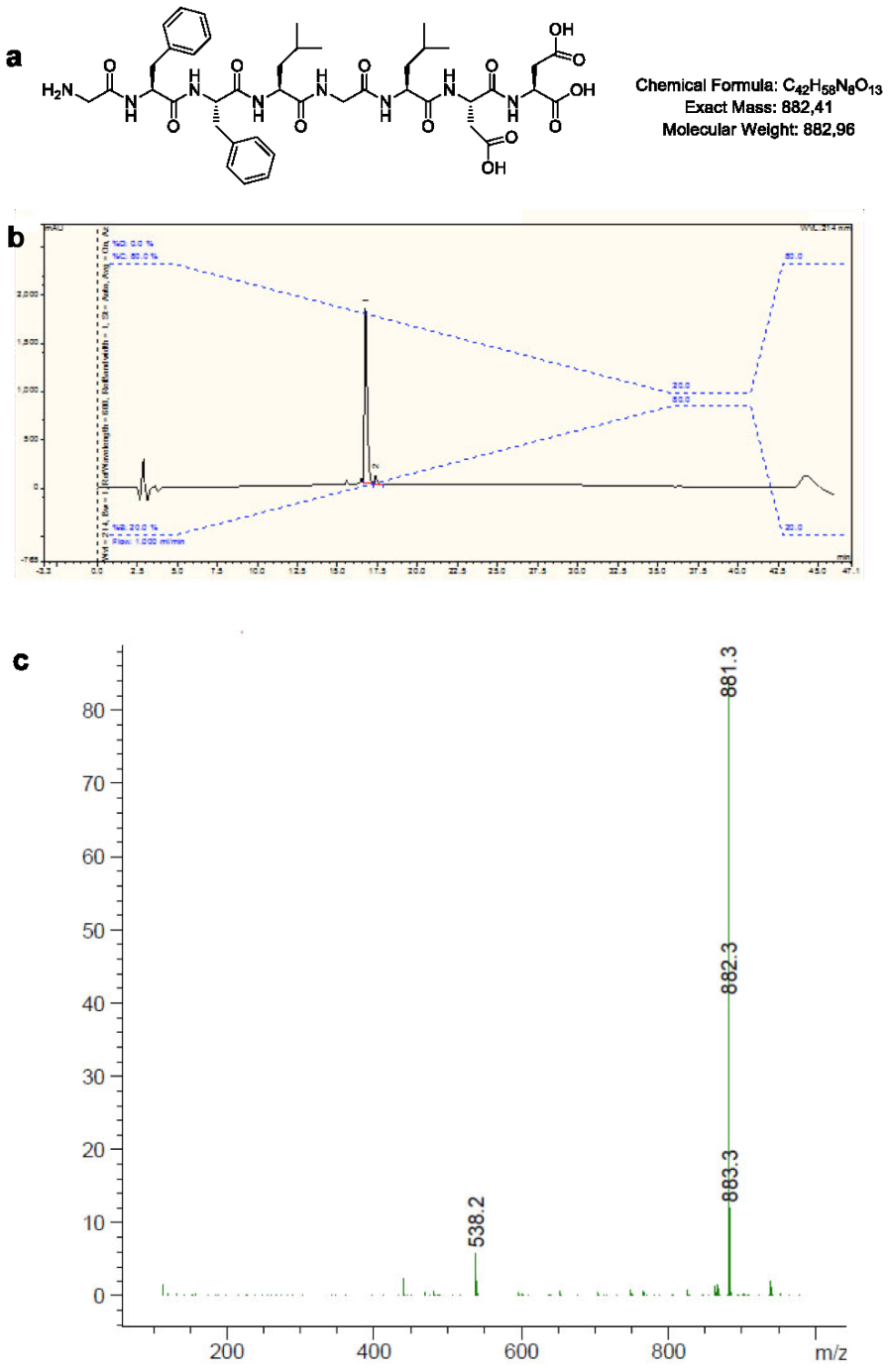

Figure S 1. **Peptide synthesis and characterization of 2a.** (**a**) chemical structure of **2a** with mass analysis. (**b**) **2a** peptide sequence was analyzed by HPLC (20-80% Solvent B) and shows a retention time of 16.8 min. (**c**) LCMS results are as follows: LC (5-100% Solvent D, retention time =10.1 min) and MS (mass calculated: $[M-H]^-$= 881.4, mass observed: $[M-H]^-$ = 881.3).

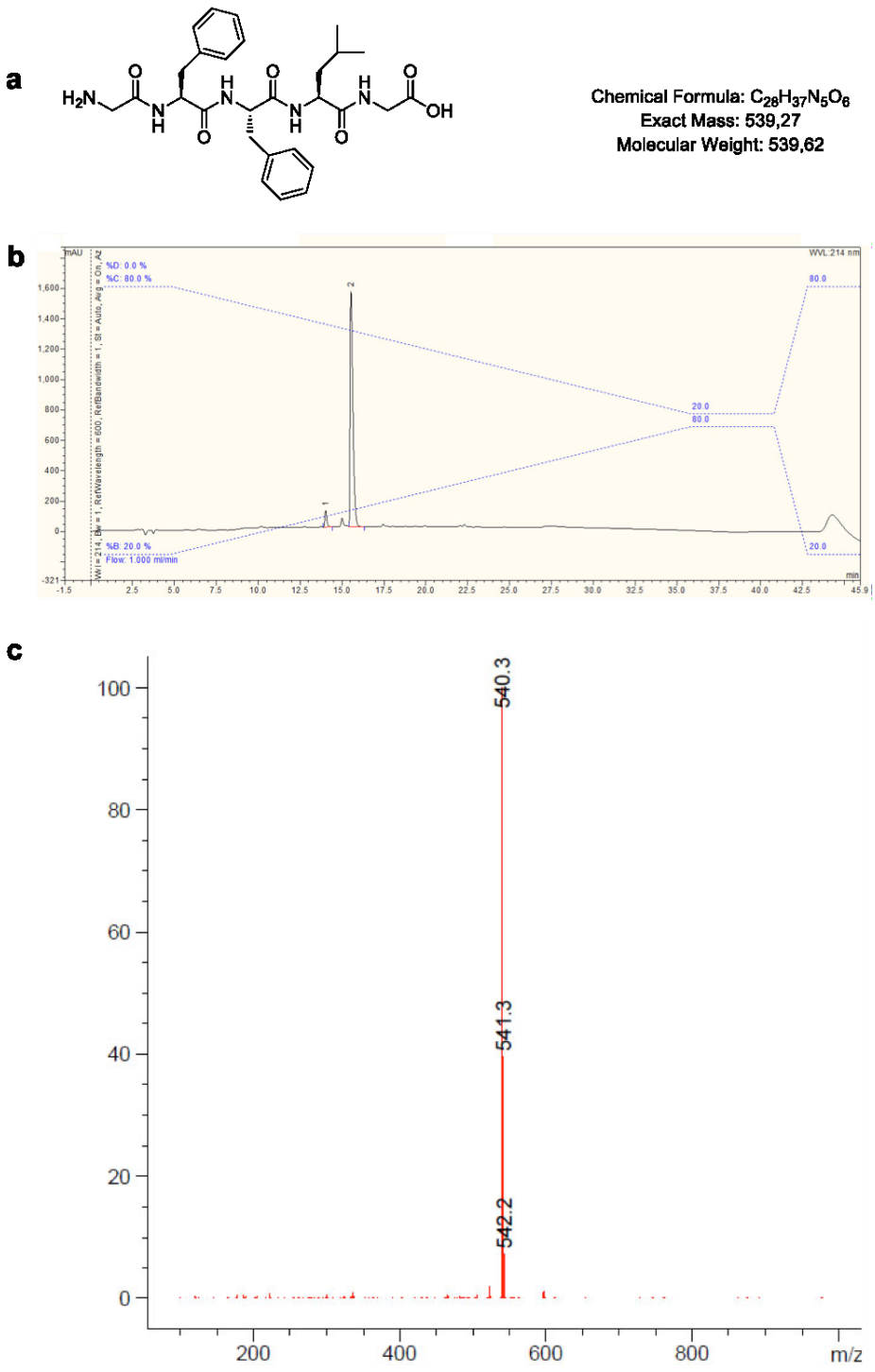

Figure S 2. **Peptide synthesis and characterization of 2b.** (**a**) chemical structure of **2b** with mass analysis. (**b**) **2b** peptide sequence was analyzed by HPLC (20-80% Solvent B) and shows a retention time of 15.6 min. (**c**) LCMS results are as follows: LC (5-100% Solvent D, retention time = 10.1 min) and MS (mass calculated: $[M+H]^+$= 540.3, mass observed: $[M+H]^+$ = 540.3).

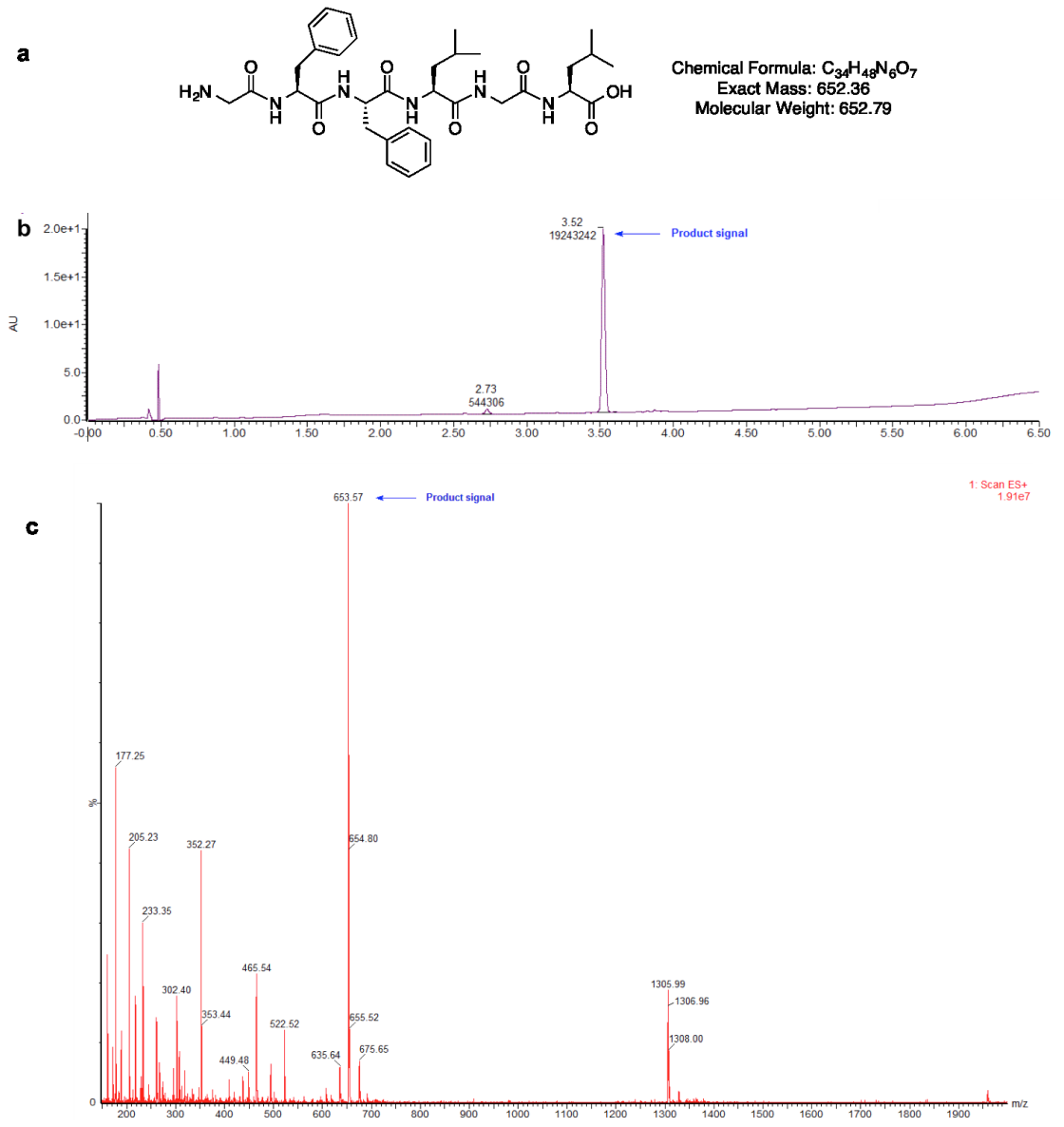

Figure S 3. **Peptide synthesis and characterization of 2c.** (**a**) chemical structure of **2c** with mass analysis. (**b**) UPLC (data provided by CEM) results are as follows: retention time = 3.5 min and (**c**) MS (mass calculated: $[M+H]^+$= 653.3, mass observed: $[M+H]^+$ = 653.5).

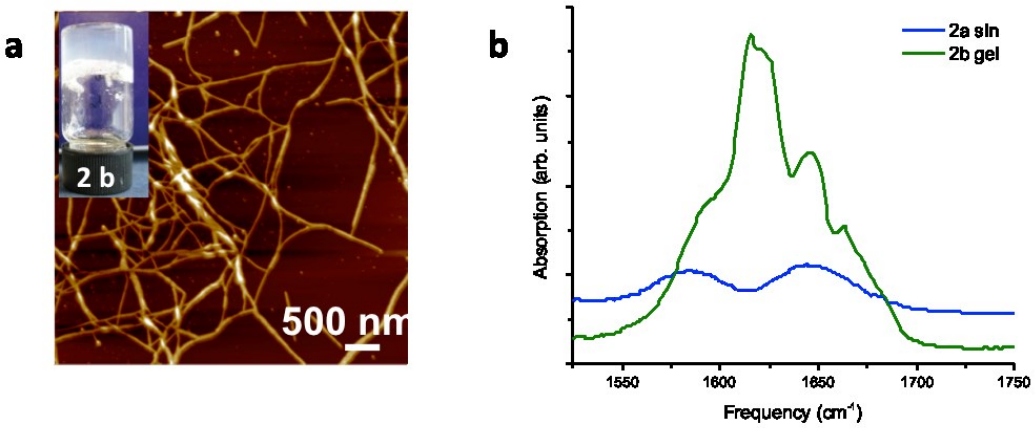

Figure S 4. Self-assembly characterization of 2b. (**a**) Atomic force microscopy (AFM) showing fibres (hydrogels – 20 mM) for **2b**. (**b)** FTIR absorption spectrum in the amide I region (in D_2O at pH 7): **2a** (solution) and **2b** (gel).

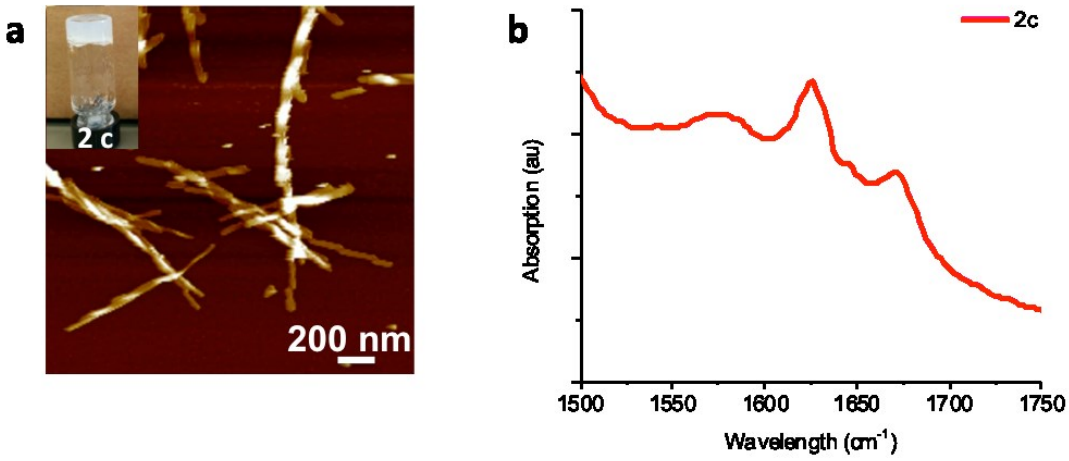

Figure S 5. Self-assembly characterization of 2c. (a) AFM showing fibres for hydrogels (20 mM) for **2c**. (**b**) FTIR absorption spectrum in the amide I region (D_2O, pH 7) for **2c** gel.

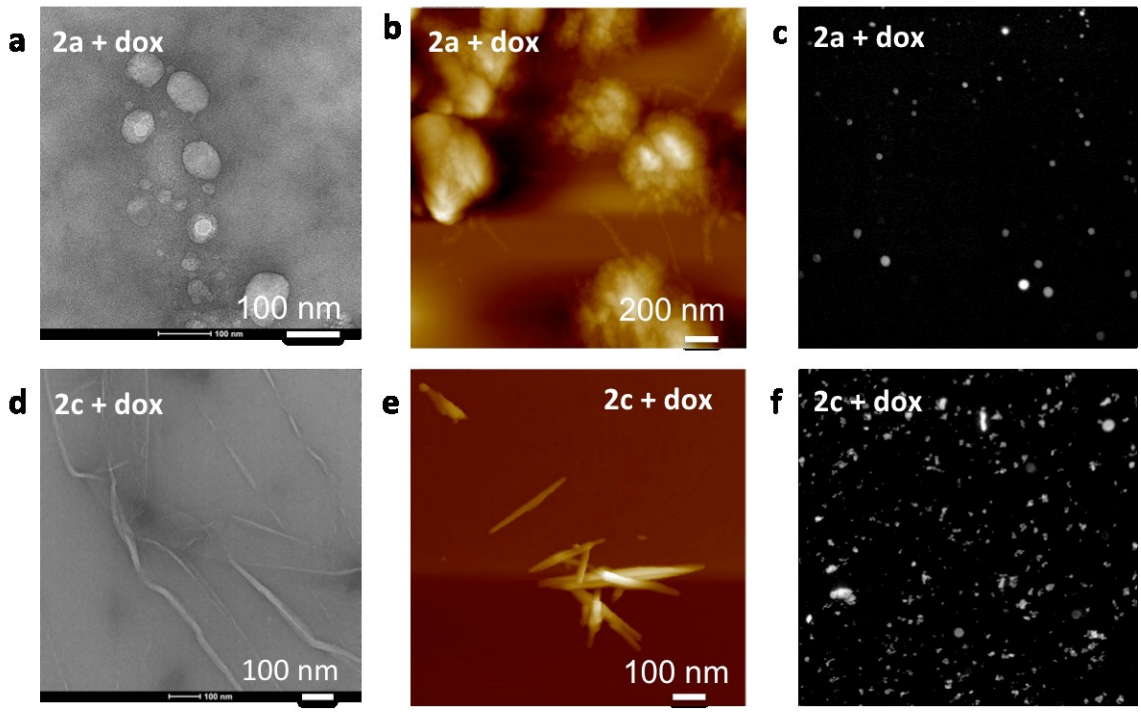

Figure S 6. Self-assembly characterization in presence of doxorubicin. (**a**) TEM, (**b**) AFM and (**c**) fluorescence microscopy (magnification 10x) images of doxorubicin loaded octapeptide (**2a**) showing that micelle formation was not disrupted by the presence of the drug (doxorubicin) and that the doxorubicin (fluorescence microscopy) is retained in the micelles. (**d**) TEM and (**e**) AFM showing the synthetically made observed cleavage product (**2c**) confirming fibers are forming in presence of doxorubicin and (**f**) fluorescence microscopy (magnification 10x) showing doxorubicin entrapment in the fibers.

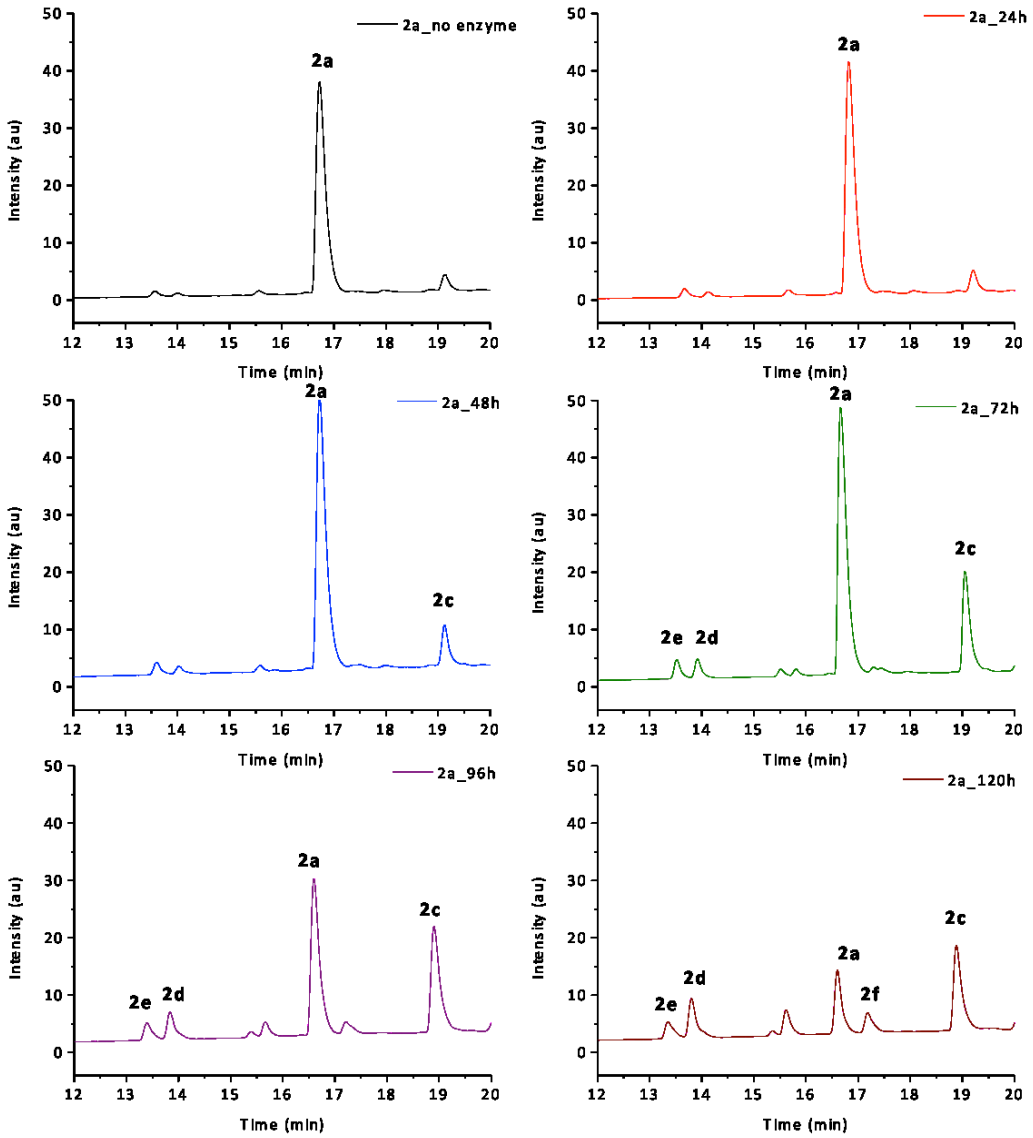

Figure S 7. HPLC of peptide (2a) digestion with MMP-9. HPLC chromatograms showing the MMP-9 induced digestion of **2a** monitored over 120 h. Product formation at different time points is showed: time 0 (no enzyme), 24 h, 48 h. 72 h, 96 h and 120 h. More in detail, GFFLGLDD is converted to 3 main products after 96 h: GFFLGL (2c): HPLC (20-80% Solvent B, retention time = 18.9 min). LCMS: LC (5-100% Solvent D, retention time = 10.3 min), MS (mass calculated: $[M-H]^-$= 651.3, mass observed: $[M-H]^-$ = 651.3); GFF (2d): HPLC (20-80% Solvent B, retention time = 14.1 min). LCMS: LC (5-100% Solvent D, retention time = 8.6 min), MS (mass calculated: $[M-H]^-$= 368.1, mass observed: $[M-H]^-$ = 368.1); FLGLDD (2e): HPLC (20-80% Solvent B, retention time = 13.7 min). LCMS: LC (5-100% Solvent D, retention time = 8.5 min), MS (mass calculated: $[M+H]^+$= 679.3, mass observed: $[M+H]^+$ = 679.3). After 120 h further fragmentation of the substrate is observed, but also the digestion of the GFFLGL product (2c) into GF and FLGL (2f): HPLC (20-80% Solvent B, retention time = 17.2 min).

LCMS: LC (5-100% Solvent D, retention time = 9.3 min), MS (mass calculated: $[M-H]^-$ = 447.2, mass observed: $[M-H]^-$ = 447.1)

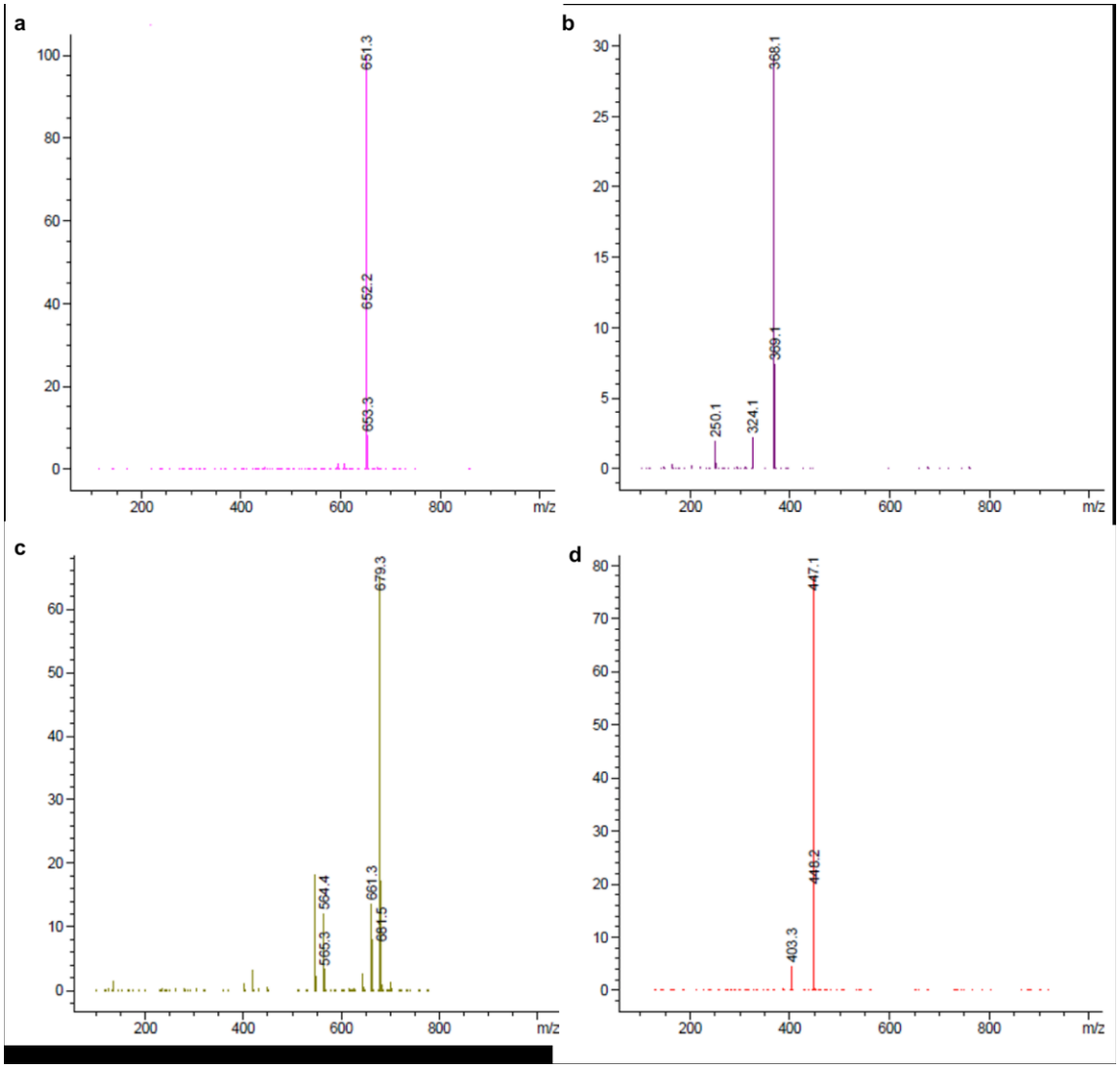

Figure S 8. Mass spectra of peptide (2a) digestion with MMP-9. MS data for (**a**) GFFLGL (**2c**), (**b**) GFF (**2d**), (**c**) FLGLDD (**2e**) and (**d**) FLGL (**2f**) described in the previous figure (Supplementary Figure 7).

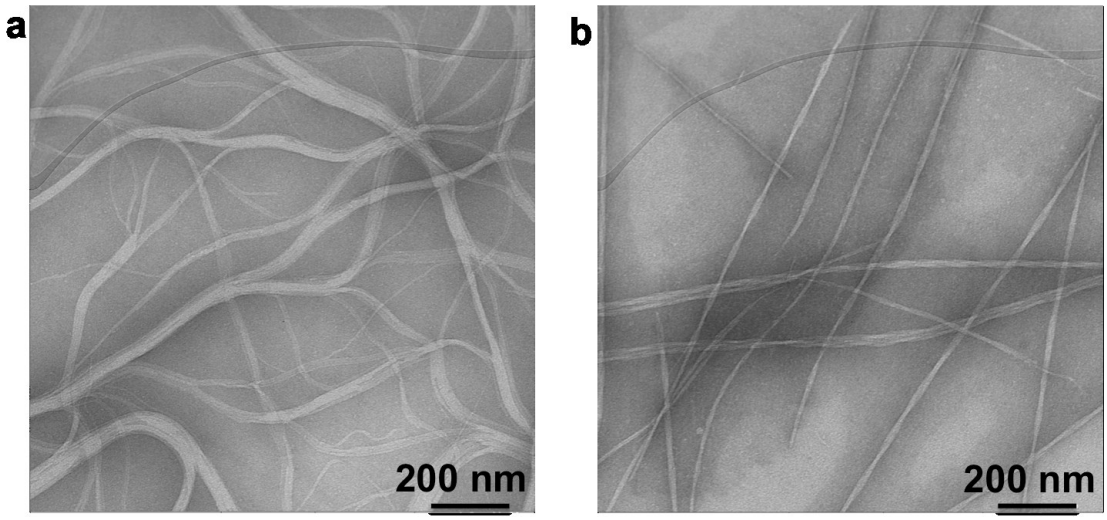

Figure S 9. TEM images. (**a**) **1a** and (**b**) **2a** treated with MMP-9 for 96 h to form fibers of **1c** and **2c**, respectively.

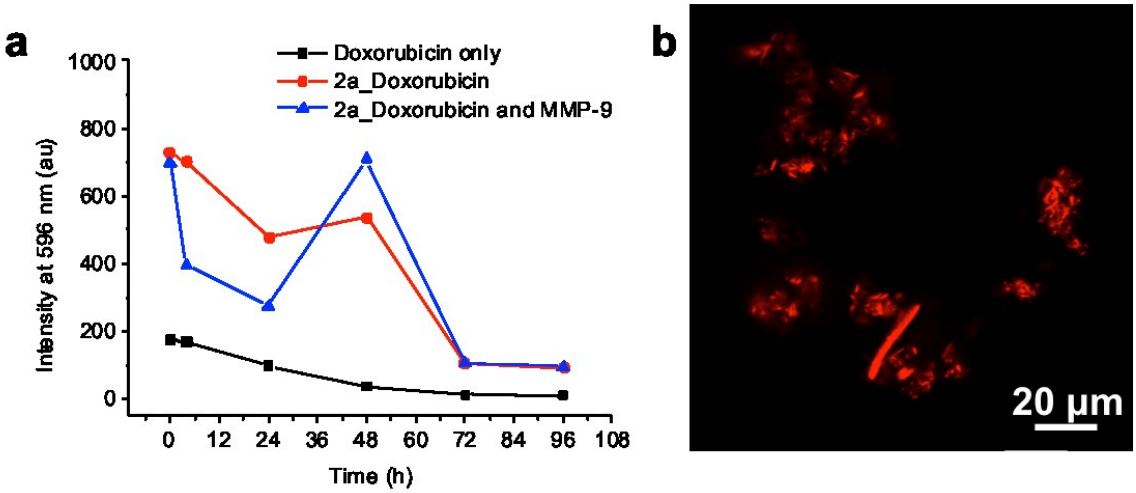

Figure S 10. Doxorubicin fluorescence. (**a**) Fluorescence intensities of doxorubicin monitored over time for doxorubicin only, doxorubicin loaded into precursor peptide (**2a**) micelles and MMP-9 treated precursor peptide (**2a**) micelles loaded with doxorubicin. (**b**) Confocal microscopy after MMP-9 treatment confirming that the doxorubicin is trapped in the peptide fibers.

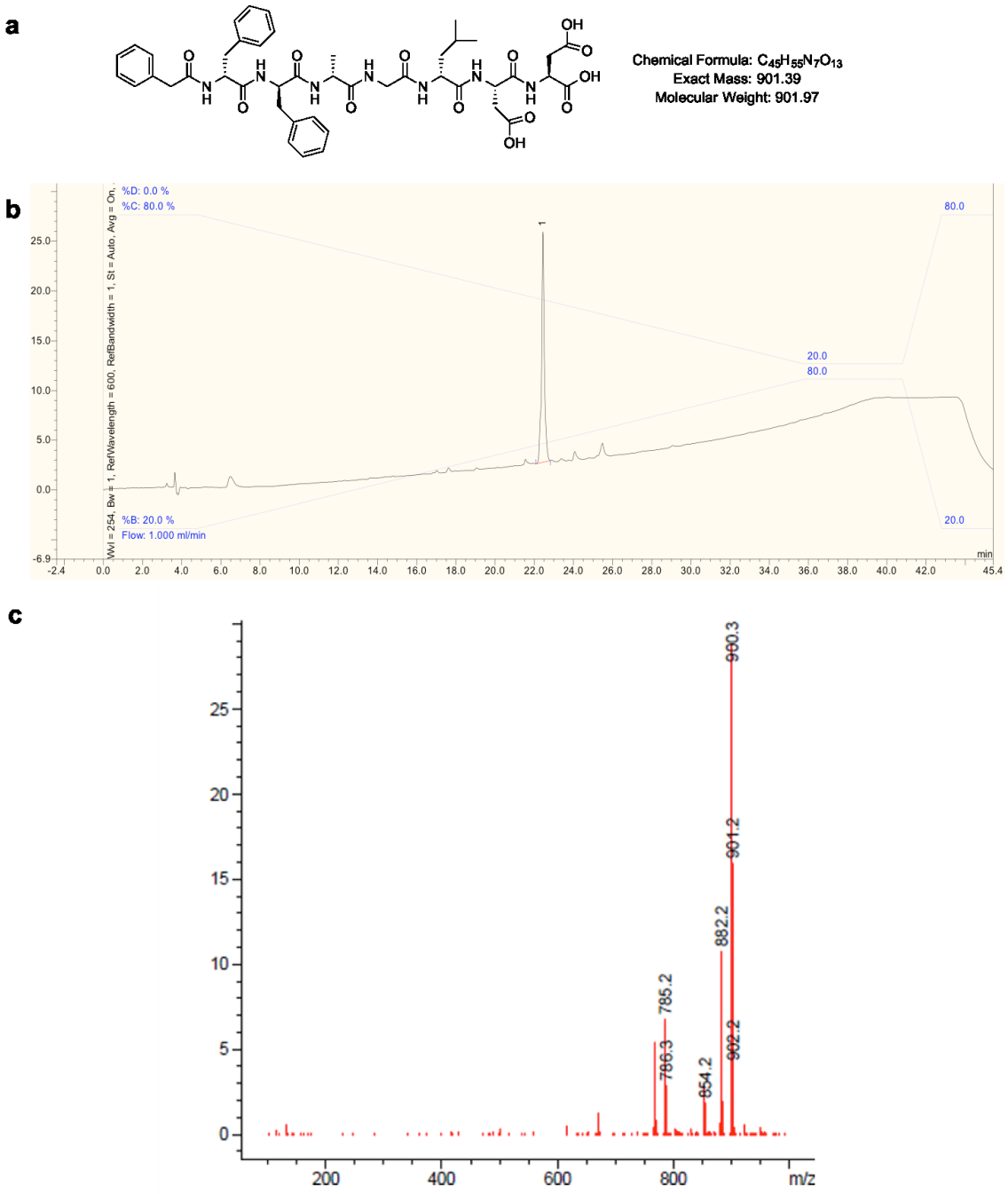

Figure S 11. Peptide synthesis and characterization of 1a(D). (**a**) chemical structure of **1a(D)** with mass analysis. (**b**) **1a(D)** peptide sequence was analyzed by HPLC (20-80% Solvent B) and shows a retention time of 22.5 min. (**c**) MS (mass calculated: $[M-H]^-$= 900.4, mass observed: $[M-H]^-$ = 900.3).

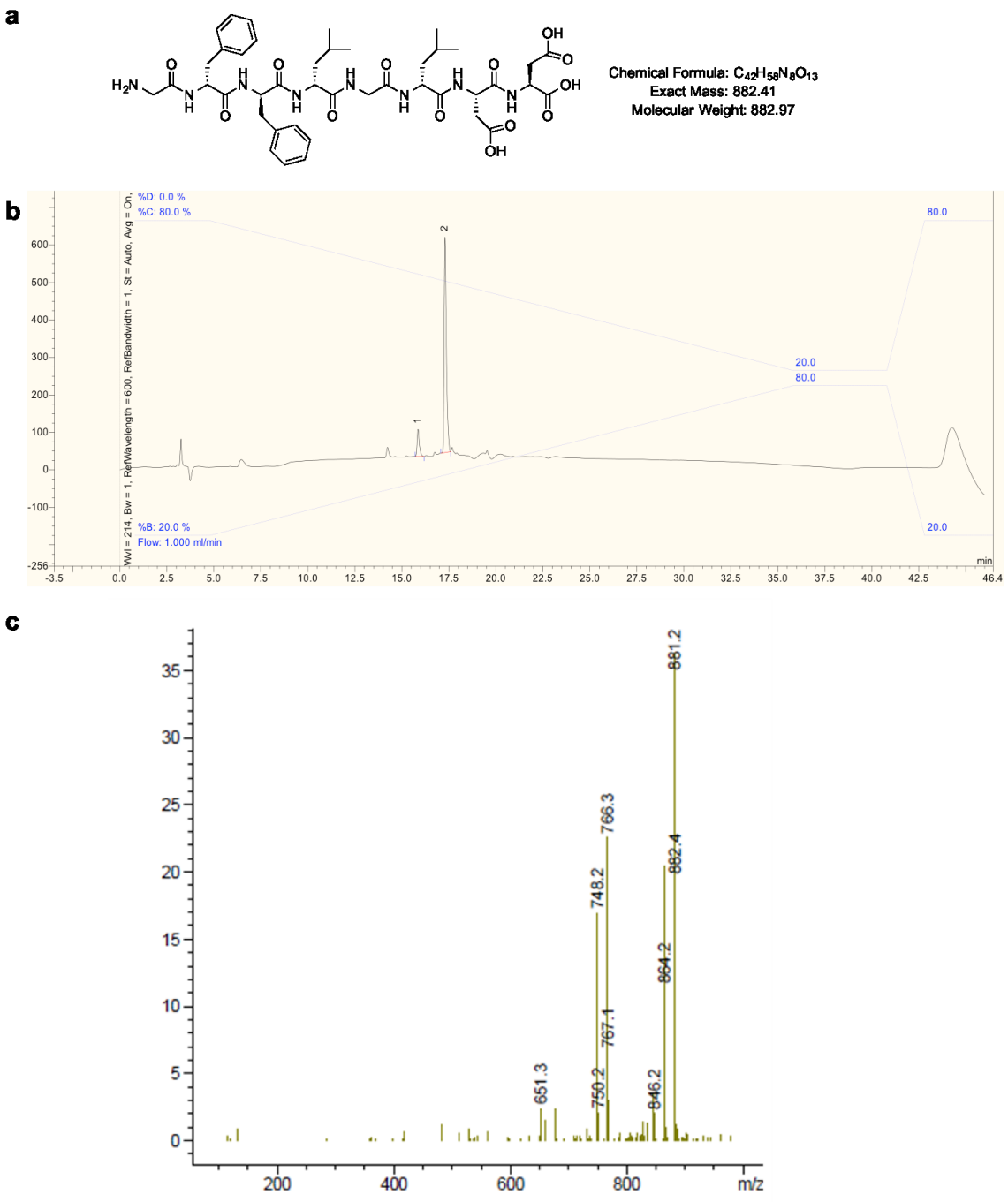

Figure S 12. Peptide synthesis and characterization of 2a(D). (**a**) chemical structure of **2a(D)** with mass analysis. (**b**) **2a(D)** peptide sequence was analyzed by HPLC (20-80% Solvent B) and shows a retention time of 17.5 min. (**c**) MS (mass calculated: $[M-H]^-$= 881.4, mass observed: $[M-H]^-$ = 881.2).

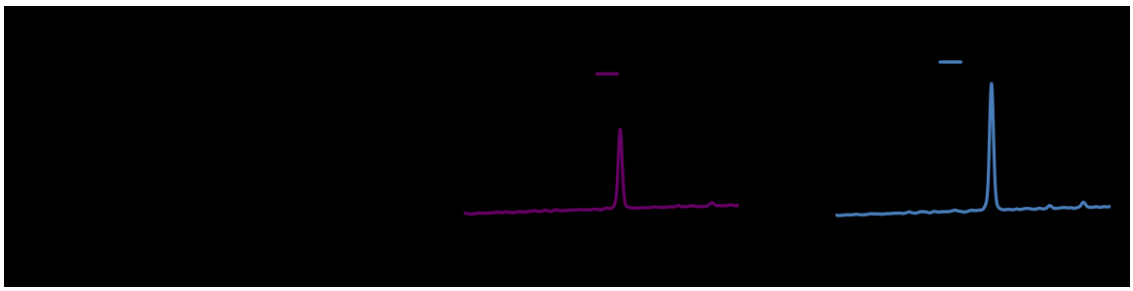

Figure S 13. HPLC of peptide 1a D treated with MMP-9 for 10 days to assess stability. HPLC chromatograms showing the resistance of **1a D** to MMP-9 digestion monitored at **(a)** time 0 (no enzyme), **(b)** 96 h and **(c)** 240 h. **1a (D)** peptide sequence was analyzed by HPLC (30-50% Solvent B, 70 min) and shows a retention time of 35.1 min for all three time points.

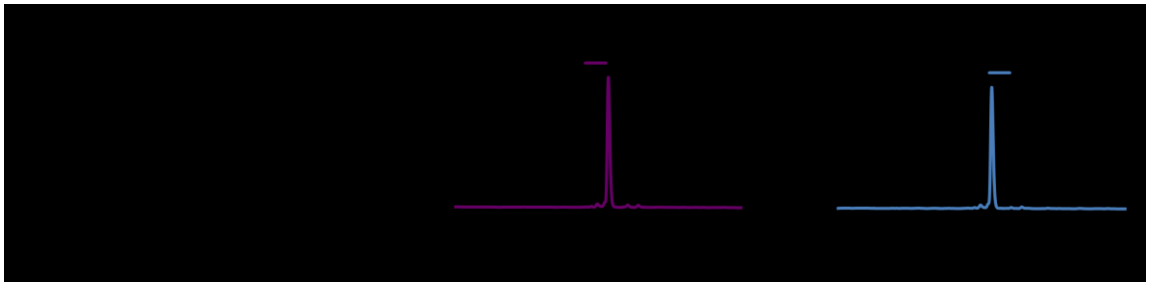

Figure S 14. HPLC of peptide 2a D treated with MMP-9 for 10 days to assess stability. HPLC chromatograms showing the resistance of **2a D** to MMP-9 digestion monitored at **(a)** time 0 (no enzyme), **(b)** 96 h and **(c)** 240 h. **2a (D)** peptide sequence was analyzed by HPLC (20-80% Solvent B, 45 min) and shows a retention time of 17.5 min for all three time points.

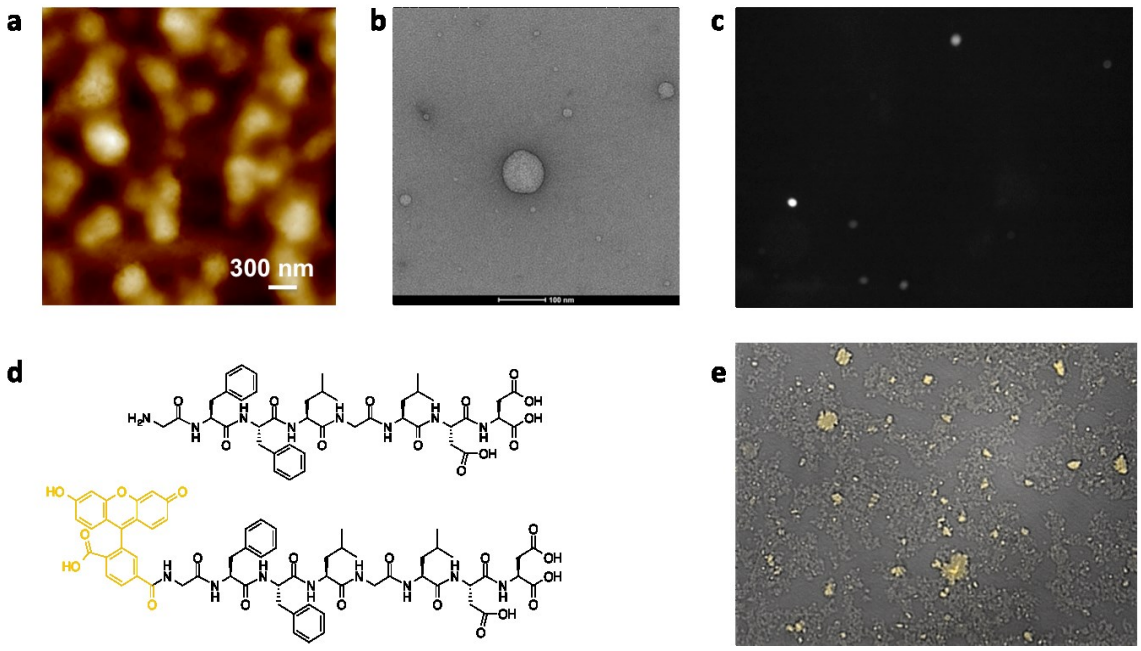

Figure S 15. Co-assembly of 2a with 1% of carboxyfluorescein-2a for visualization. In order to visualize the peptide distribution in presence of cells, the co-assembly of 2a with 1% of carboxyfluorescein-2a was studied and characterized by AFM, TEM and fluorescence microscopy. **(a)** AFM, **(b)** TEM (scale bar: 100 nm), **(c)** and **(e)** fluorescence microscopy (magnification 10x) of the co-assembled structures formed by mixing of **2a** and carboxyfluorescein-**2a**. **(d)** Chemical structures of **2a** and carboxyfluorescein-**2a**.

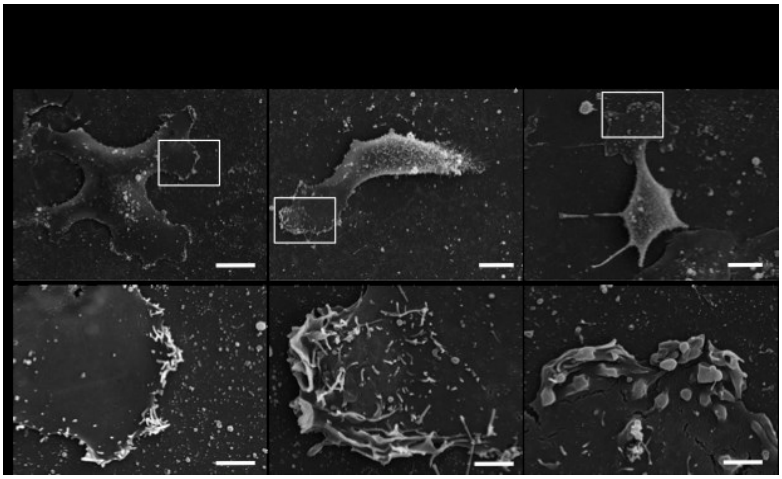

Figure S 16. Effect of the MMP-9 cleavable peptide 2a on cell morphology *in vitro*. Altered lamellipodia morphology upon PMA stimulation after 3 day treatment with 2.5 mM of peptide **2a (D)** or **2a** visualized by SEM; top panel, bar: 10 μm; lower panel magnified selected region, bar: 2 μm.

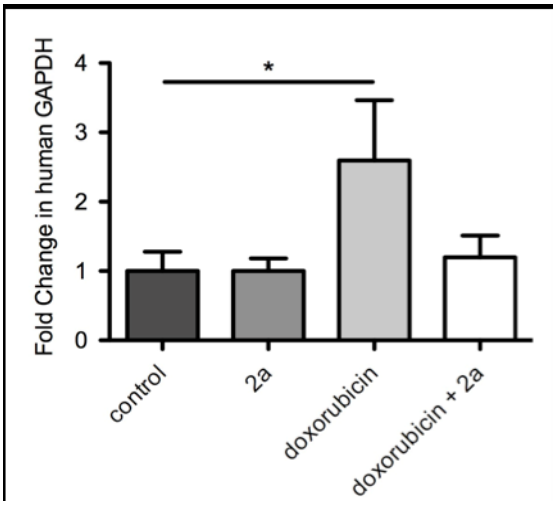

Figure S 17. MMP-9 cleavable peptide carrier 2a rescues effect of doxorubicin treatment on circulating tumor cells. A Quantification of circulating tumor cells in the blood of subcutaneous tumor bearing nude mice by RT-PCR, measuring human GAPDH levels normalized to murine beta-2-microglobulin; bars: mean of fold change. Error bars: SEM; n = 3-4 mice; * $p < 0.05$ by standard student's *t*-test.

Supplementary methods

High-performance liquid chromatography. HPLC analyses of peptides were performed using Dionex P680 HPLC system equipped with a Macherey-Nagel C18 column of 250 mm length, 4.6 mm internal diameter and 5 mm particle size equipped with UV-Vis detector. The gradient: (Solvent A: 0.1% TFA in water; Solvent B: 0.1% TFA in acetonitrile) 20-80% B was utilized, with each run lasting a total of 46 minutes using a flow rate of 1 mL min^{-1} and detection wavelengths set at 214 nm and 254 nm using the UV-Vis detector. For separation of peptides **1a** and **1c** a 30-50% B gradient was utilized with each run lasting a total of 70 minutes using a flow rate of 1 mL min^{-1} and detection wavelengths set at 214 nm and 254 nm using the UV-Vis detector.

Liquid chromatography-mass spectrometry. LC-MS obtained at the University of Strathclyde Mass Spectrometry facility was used to confirm peptide molecular weights. All analyses were carried out on a reverse-phase 15 cm Kinetex C18, 150 x 4.6 mm, 5 micron column. The LC-MS instrument was an Agilent 1200 Series HPLC, coupled to an Agilent 6130 Dual source MS detector. The gradient: (Solvent C: 5 mM ammonium acetate in water; Solvent D: 5 mM ammonium acetate in acetonitrile) 0-3 min 5% D, 3-17 min 5-100% D, 17-27 min 100% D, 27-33 min 100-5% D, and 33-36 min 5% D was used in all analyses; the flow rate was set at 1 mL min^{-1} and detection wavelengths at 214 nm. Mass detection was set to analyse in Scan mode with electrospray ionisation (MM-ES+APCI). For all peptides examined both positive and negative ions were detected but only one (positive or negative ion) is shown for peptide characterisation to avoid redundancy.

Fourier Transform Infrared Spectroscopy. FTIR spectra were recorded on a Bruker Vertex 70 spectrometer. Samples were prepared in deuterated phosphate buffer (pH=8) and placed between two CaF_2 cells with 12mm diameter polytetrafluoroethylene (PTFE) spacers. Absorbance spectra were taken from 4000cm^{-1} to 800cm^{-1} with 64 scans at 4cm^{-1} resolution.

Fluorescent microscope images were captured on the GE Cytell Imaging System using the Digital Imaging program. Samples were prepared on a standard glass slide and an 18x18mm micro cover glass was placed on top. Pictures were taken at 2000-2500 focus (micron).

Doxorubicin encapsulation. Doxorubicin hydrochloride was solubilized in DMSO by sonication and 1 mM stock solution was made in PBS was made and subsequently diluted into the suspension of peptide micelles (final concentration of doxorubicin: 5 μM). The samples were then sonicated to allow doxorubicin diffusion into the hydrophobic core of the micelles. Fluorescence intensity of doxorubicin at 596 nm that corresponds to the maximum intensity (λ_{ex} = 480 nm) was monitored over 96 h when incorporated into the **2a** peptide system with and without addition of MMP-9. A control experiment with free doxorubicin (doxorubicin in water, no peptide present) shows a low fluorescence intensity as previously reported (more intense fluorescence signal of doxorubicin is observed in hydrophobic environment compared to water- as fluorescence intensity changes with the polarity of the environment).[1,2]

Fluorescence emission spectra were measured on a Jasco FP-6500 spectrofluorometer. Doxorubicin was excited at 480 nm and the emission intensity at 596 nm was monitored over time. The excitation and emission bandwidths were both set to 5 nm.

CRISPR sequences.

MMP-9 CRISPR-for	CACCGTGTACCGCTATGGTTACACT	primer for CRISPR of human MMP-9, Exon 1, 93%
MMP-9 CRISPR-rev	AAACAGTGTAACCATAGCGGTACAC	Primer for CRISPR of human MMP-9, Exon 1, 93%

Quantification of circulating tumor cells. Circulating tumor cells were detected as described previously[3,4], briefly 500 μL of blood was collected by cardiac puncture, snap frozen and kept at -70C. RNA was isolated using the Ambion Mouse RiboPure™-Blood RNA Isolation Kit (AM1951, Applied Biosystems) and ~ 1 μg used for cDNA synthesis using SuperScript™ kit (ThermoFisher Scientific, Life Technologies). Using qPCR

SYBR®Green (ThermoFisher Scientific) the levels of human GAPDH were quantified after normalization to murine beta-2-microglobulin, using the comparative C(t) value method[5].

(1) Hughes, M.; Birchall, L. S.; Zuberi, K.; Aitken, L. a.; Debnath, S.; Javid, N.; Ulijn, R. V. Differential Supramolecular Organisation of Fmoc-Dipeptides with Hydrophilic Terminal Amino Acid Residues by Biocatalytic Self-Assembly. *Soft Matter* **2012**, *8*, 11565.

(2) Kalafatovic, D.; Nobis, M.; Javid, N.; Frederix, P. W. J. M.; Anderson, K. I.; Saunders, B. R.; Ulijn, R. V. MMP-9 Triggered Micelle-to-Fibre Transitions for Slow Release of Doxorubicin. *Biomater. Sci.* **2015**, *3*, 246–249.

(3) Padua, D.; Zhang, X. H.-F.; Wang, Q.; Nadal, C.; Gerald, W. L.; Gomis, R. R.; Massagué, J. TGFbeta Primes Breast Tumors for Lung Metastasis Seeding through Angiopoietin-like 4. *Cell* **2008**, *133*, 66–77.

(4) Gupta, G. P.; Nguyen, D. X.; Chiang, A. C.; Bos, P. D.; Kim, J. Y.; Nadal, C.; Gomis, R. R.; Manova-Todorova, K.; Massagué, J. Mediators of Vascular Remodelling Co-Opted for Sequential Steps in Lung Metastasis. *Nature* **2007**, *446*, 765–770.

(5) Schmittgen, T. D.; Livak, K. J. Analyzing Real-Time PCR Data by the Comparative CT Method. *Nat. Protoc.* **2008**, *3*, 1101–1108.